5-20-2021

Variability of USA East Coast surface total alkalinity distributions revealed by automated instrument measurements

Christopher W. Hunt
University of New Hampshire, Christopher.Hunt@unh.edu

Joseph Salisbury
University of New Hampshire

Douglas Vandemark
University of New Hampshire, Durham

Steffen Aßmann

Christopher Melrose
NOAA Fisheries, chris.melrose@noaa.gov

See next page for additional authors

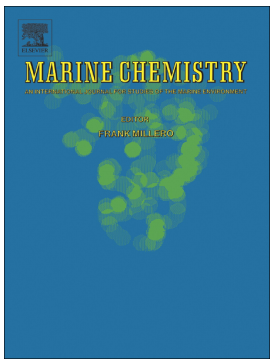

Variability of USA East Coast surface total alkalinity distributions revealed by automated instrument measurements

Christopher W. Hunt, Joseph E. Salisbury, Douglas Vandemark, Steffen Aßmann, Peer Fietzek, Christopher Melrose, Rik Wanninkhof, Kumiko Azetsu-Scott

PII: S0304-4203(21)00045-1

DOI: https://doi.org/10.1016/j.marchem.2021.103960

Reference: MARCHE 103960

To appear in: *Marine Chemistry*

Received date: 19 June 2020

Revised date: 26 January 2021

Accepted date: 7 February 2021

Please cite this article as: C.W. Hunt, J.E. Salisbury, D. Vandemark, et al., Variability of USA East Coast surface total alkalinity distributions revealed by automated instrument measurements, *Marine Chemistry* (2019), https://doi.org/10.1016/j.marchem.2021.103960

Variability of USA East Coast Surface Total Alkalinity Distributions Revealed by Automated Instrument Measurements

Christopher W. Hunt[a,*], Joseph E. Salisbury[a], Douglas Vandemark[a], Steffen Aßmann[b], Peer Fietzek[c], Christopher Melrose[d], Rik Wanninkhof[e], Kumiko Azetsu-Scott[f]

a Ocean Process Analysis Laboratory, University of New Hampshire, Durham NH USA

b formerly of Kongsberg Maritime Contros GmbH, Kiel Germany

c Kongsberg Maritime GmbH, Hamburg Germany

d NOAA Northeast Fisheries Science Center, Narragansett, RI USA

e NOAA Atlantic Oceanographic and Meteorological Laboratory, Miami FL USA

f Fisheries and Oceans, Canada, Bedford Institute of Oceanography, Dartmouth, NS, Canada

**chunt@unh.edu*

keywords: total alkalinity, Atlantic Ocean, USA, East Coast, surface water, coastal

Abstract

Seawater total alkalinity (TA) is one important determinant used to monitor the ocean carbon cycle, whose spatial distributions have previously been characterized along the United States East Coast via discrete bottle samples. Using these data, several regional models for TA retrievals based on practical salinity (S) have been developed. Broad-scale seasonal or interannual variations, however, are not well resolved in these models and existing data are highly seasonally biased. This study reports findings from the first long duration deployment of a new, commercially available TA titrator aboard a research vessel and the continuous underway surface TA measurements produced. The instrument, operated on seven East Coast USA cruises during six months in 2017 and for two months in 2018 on the summertime East Coast Ocean Acidification survey (ECOA-2), collected a total of nearly 11,000 surface TA measurements. Data from these efforts, along with a newly synthesized set of more than 11,000 regional surface TA observations, are analyzed to re-examine distributions of TA and S along the United States East Coast. Overall, regional distributions of S and TA generally agreed with prior findings, but linear TA:S regressions varied markedly over time and deviated from previously developed models. This variability is likely due to a combination of biological, seasonal, and episodic influences and indicates that substantial errors of ±10-20 µmol kg^{-1} in TA estimation from S can be expected due to these factors. This finding has likely implications for numerical ecosystem modeling and inorganic carbon system calculations. New results presented in this paper provide refined surface TA:S relationships, present more data in space and time, and improve TA modeling uncertainty.

Introduction

The important role of ocean alkalinity in regulating climate has become more apparent in recent years, as oceans are estimated to have absorbed about 25% of anthropogenic carbon dioxide (CO_2)

between 2006-2015 (Friedlingstein et al. 2019). Waters containing higher alkalinity concentration relative to CO_2 provide enhanced buffering and CO_2 sequestration potential. This sequestration has led to a decrease in global upper ocean pH by about 0.002 yr^{-1} (Feely et al. 2004, Doney et al. 2011), a process termed ocean acidification (OA). Vast stores of alkalinity in deep ocean waters represent more than enough neutralizing capacity to mitigate anthropogenic OA over millennial time scales (Zeebe 2012). Over decadal time scales, the less-buffered upper ocean and coastal waters, where high biological production occurs, are more susceptible to OA and its consequences. Coastal areas may be especially vulnerable to the impacts of OA (Mathis et al. 2015, Breitburg et al. 2015), but the dynamics of OA and buffering capacity in these areas are still poorly understood relative to the open ocean. This is due to the complex interplay between a number of additional coastal biogeochemical and physical processes, including biological calcium carbonate production and dissolution (Cross et al. 2013), anaerobic alkalinity generation (Thomas et al. 2009), river inputs (Salisbury et al. 2008), intertidal marsh exchanges (Wang et al. 2016), bottom-water acidification from metabolic CO_2 accumulation (Cai et al. 2011, Mucci et al. 2011), as well as cross-shelf exchange (Chen and Wang 1999). These processes, combined with the large range of variability in coastal ocean alkalinity, pH, and hydrography, can lead to substantial uncertainties in ecosystem models used to predict future OA impacts in these areas (Wallace et al. 2014, Hagens et al. 2015, Breitburg et al. 2015).

TA and dissolved inorganic carbon (DIC) distributions along the United States East Coast ocean margin (henceforth shortened to East Coast) have been extensively studied during several transects, including the four GOMECC (Gulf of Mexico and East Coast Carbon) and ECOA (East Coast Ocean Acidification) cruises (Cai et al. 2010, Wang et al. 2013, Wanninkhof et al. 2015) and the Ocean Margins Program in the MAB (Chipman et al. 1995). These ongoing surveys provide a synoptic view of conditions in the region, but they were confined to the summer season, were resource- and labor-intensive, and were spaced several years apart. Methods that can expand temporal and spatial coverage of inorganic

carbon system parameters would greatly enhance model estimates of East Coast DIC and CO_2 exchange (Signorini et al. 2013).

Recent developments in both ocean observation and data synthesis efforts offer the promise of vastly improved East Coast TA and inorganic carbon estimates. In-situ data compilations such as GLODAP (Olsen et al. 2016, Key et al. 2015) provide extensive collections of in-situ TA, DIC, and pH measurements. These datasets have been used to construct statistical relationships between TA and practical salinity (hereafter referred to as "salinity" in this work and abbreviated as "S") and sometimes temperature for major ocean basins (Lee et al. 2006, Millero et al. 1998, Takahashi et al. 2014), smaller sub-basins (Takahashi et al. 2014, Jiang et al. 2014, Cross et al. 2013), and even segmented coastal areas (DeGrandpre et al. 1997, Cai et al. 2010, Joesoef et al. 2017). In particular, Millero et al. (1998) presented an 'Atlantic' relationship assembled using surface data from 60°S to 80°N, whereas Lee et al. (2006) presented a 'North Atlantic' relationship using data from 30°N to 80°N.

These relationships have been used to estimate TA from either *in situ* salinity observations, salinity climatologies (Zweng et al. 2019), or space-based satellite measurements (Signorini et al. 2013, Fine et al. 2017, Salisbury and Jönsson 2018, Land et al. 2019, Reul et al. 2020). Satellite missions offer the potential for synoptic salinity estimates over vast spatial scales (Salisbury et al. 2015, Grodsky et al. 2018), which can then be used to derive estimates of surface ocean TA. The statistical relationships used to produce these estimates are, however, regionally and temporally variable (e.g. Land et al. 2019, Cai et al. 2010, Li et al. 2020). An additional source of high-quality TA data for the USA East Coast, collected at a higher frequency than the three-to-five year interval of the previous GOMECC/ECOA cruises, could inform the temporally variable nature of regional relationships. Recent technological advances and development efforts have provided a commercially available tool for this purpose: an automated TA analyzer (the CONTROS HydroFIA® TA, -4H-JENA Engineering GmbH, Jena, Germany, formerly of Kongsberg Maritime Contros GmbH, Kiel, Germany, hereafter referenced as HydroFIA TA). Deployed

aboard a ship of opportunity, the collected underway surface TA measurements allow us to re-examine regional TA distributions along the East Coast and test existing statistical models relating salinity to TA. Here, we evaluate the performance of the HydroFIA TA instrument on multiple cruises aboard a ship of opportunity, present recommendations for future deployments, compare findings to previous studies as well as to a newly-assembled database of historical East Coast TA measurements, and discuss how data collected during this effort help to inform our understanding of TA variability along the East Coast.

Methods

Study Regions

This study reports on observations from four East Coast oceanographic regions: Gulf of Maine, Nantucket Shoals/George's Bank, Middle Atlantic Bight, and offshore Shelf Break Front (Figure 1). Delineations of the boundaries between these regions follow the methods of Signorini et al. (2013) and Hofmann et al. (2008). The Gulf of Maine (GOM, Figure 1) is a highly productive, semi-enclosed shelf sea, encompassing the area between Cape Cod in Massachusetts and the Canadian province of Nova Scotia. The area east of the Scotian shelf and also east of the more northern Newfoundland and Labrador shelf system is where the warm, salty, northeast-flowing Gulf Stream and the colder, fresher, southwest-flowing Labrador Current interact (Loder et al. 1998). GOM circulation is typically cyclonic, with upstream Scotian Shelf and Atlantic slope water entering the region through the Northeast Channel and across the western Scotian Shelf, following the Maine coast southward, and exiting the GOM around the eastern flank of George's Bank and the Great South Channel between the Nantucket and George's Bank shoals. The area of George's Bank and Nantucket Shoals (GBN) comprises two shallow regions which together geographically separate the GOM from the Middle Atlantic Bight, bisected north-to-south by the Great South Channel. This region supports an active commercial fishery. The Middle

Atlantic Bight (MAB) extends roughly from Cape Cod in Massachusetts to Cape Hatteras in North Carolina. This area also resides at the intersection of two major ocean currents: the colder, fresher inshore modified Labrador coastal current from the north (flowing first through the GOM and GBN regions) and the warmer, saltier offshore Gulf Stream from the south (Wang et al. 2013). These two currents are separated by the inshore shelf areas and slope sea further offshore, which stretches from Cape Hatteras to the Grand Banks. Warm core rings, shed from the Gulf Stream into the slope sea, are a frequent source of warm, high salinity water to the MAB region via cross-shelf exchange (Hofmann et al. 2008). The MAB is characterized by springtime phytoplankton blooms and low pCO_2 during the winter and spring months (DeGrandpre et al. 2002, Wang et al. 2013). The offshore Shelf Break Front (SBF) region delineates a band of slope sea stretching from south of Cape Hatteras northeastward nearly to Nova Scotia, encompassing the area where the seafloor deepens from several hundred meters to more than 2000 m, and forming a boundary region between the inshore GOM, GBN and MAB regions and the offshore slope sea.

Analytical Methods for Practical Salinity, Water Temperature, and pCO_2

Measurements in 2017 were collected on seven cruises of opportunity aboard the National Oceanic and Atmospheric Administration (NOAA) Ship *Henry B. Bigelow* (hereafter referred to as the *Bigelow*), a 64-meter fisheries research vessel. A summary of these cruises is provided in Table 1. Surface seawater temperature and practical salinity (hereafter referred to as salinity) were measured from a continuous surface seawater supply (intake depth about 3 m) using a Seabird SBE-45 thermosalinograph (Sea-bird Electronics, Bellevue WA, manufacturer precision of ±0.0001°C and ±0.0002, respectively). Measurements of the partial pressure of carbon dioxide (pCO_2) were made from the same continuous surface seawater supply using a General Oceanics (Miami, FL) pCO_2 measurement

system operated by the NOAA Atlantic Oceanography and Meteorological Laboratory (AOML), with a measurement accuracy of 2 µatm, as detailed in Pierrot et al. (2009).

Discrete TA Sample Collection and Analysis Methods

Discrete samples for independent instrument evaluation were collected from the ship's underway seawater supply on two cruises and analyzed by two laboratories. Samples from Cruise 1 in 2017 were collected and analyzed by the NOAA Atlantic Oceanographic and Meteorological Laboratory (AOML). Samples during the 2018 ECOA-2 cruise were analyzed by the laboratory of Dr. Wei-Jun Cai (University of Delaware, referred to hereafter as U.Del.). Water from the shipboard seawater supply was transferred without bubbling into previously-flushed 500 mL (AOML) or 250 mL (U.Del.) glass BOD bottles with greased stoppers. These were filled to leave less than 1% headspace in the bottle. Samples analyzed by AOML were preserved with 200 µl of saturated mercuric chloride solution and analyzed several weeks later; those analyzed by U.Del. were unpreserved and analyzed within 24 hours. A detailed description of the AOML TA analysis is provided by Barbero et al. (2017), specific analysis details for AOML Cruise 1 samples are described by AOML (2020), and U.Del. methods are described by Cai et al. (2010). Briefly, each lab performed open-cell titrations, measuring the e.m.f. during titration via glass pH electrodes, with results calibrated via comparison to CRM. AOML titrations were performed with 0.2N hydrochloric acid (HCl) prepared in a 0.55 molal NaCl solution. U.Del. titrations were performed with 0.1N HCl in a 0.5 molal NaCl solution. The TA endpoint of the titrations were determined according to calculation of the Gran function (Gran 1952) with a nonlinear least squares correction for the presence of sulfate and fluoride ions (Dickson et al. 2007). AOML and U.Del. instrument performance statistics are discussed below and presented in Table 2.

Analytical Method for Underway Total Alkalinity

Total Alkalinity (TA) was measured using a CONTROS HydroFIA® TA analyzer (Aßmann et al. 2013, Seelmann et al. 2019), modified for regular automated reference measurements as described below. Seelmann et al. (2019) provide a comprehensive account of instrument theory, design, and operation, and include extensive technical details we will not repeat here. Briefly, the HydroFIA TA instrument performs a single-point titration of seawater with 0.1N hydrochloric acid prepared in deionized water, using bromocresol green (BCG) as the indicator for spectrophotometric pH detection, a technique developed by Yao and Byrne (1998) and refined by Li et al. (2013).

As part of the NOAA/OTT TAACT project (Tracking Ocean Alkalinity using New Carbon Measurement Technologies), the HydroFIA TA instrument was improved to allow for the automated, periodic measurement of certified reference material (CRM) by adding CRM input and exhaust ports, liquid switching valves, and a digital controlling device connected to an external computer (Supplementary Figure S1). This capability is now a standard feature of the commercial version of the instrument. The CRM was obtained from the Scripps Institute of Oceanography laboratory of Dr. Andrew Dickson (Dickson et al. 2003), and its regular measurement supported assessments of instrument stability and accuracy over the course of multi-week deployments. Triplicate CRM measurements were typically made each day, while underway seawater TA measurements were made every 10-15 minutes. A customized software program controlled the HydroFIA TA instrument by switching between seawater and CRM sample streams, starting and stopping HydroFIA TA analysis, collecting salinity, water temperature, and location data from the ship's centralized data system, supplying real-time salinity to the HydroFIA TA analyzer, and emailing data to shoreside researchers. The HydroFIA TA instrument was serviced by NOAA personnel between each cruise, who replaced the supplies of HCl and BCG, refilled the 2l CRM reservoir (which was stoppered to limit evaporation), and re-calibrated the instrument with

CRM. After these steps, the instrument was placed in standby mode until the *Bigelow* was underway, at which time a shipboard technician used the customized software program to begin data collection.

Filtration of Underway Seawater for Total Alkalinity Analysis

Unfiltered seawater was supplied to the HydroFIA TA instrument for the first five cruises. This resulted in a steady increase in pH readings and corresponding TA readings using the same batch of CRM, presumably due to fouling of the instrument's optical cell. CRM absorbance spectra over these cruises showed decreased BCG absorbances at the isobestic point over time, which were closely correlated with increased CRM TA concentration. As the CRM TA concentration and volumes of BCG and HCl added did not change over time, we believe that accumulation of material on the optical cell resulted in increased absorbance at the indicator wavelengths. A blank spectrum measurement is made before BCG and HCl addition, and subtraction of this blank resulted in decreased calculated BCG absorbance as the blank absorbance increased. Drifts in the HydroFIA TA instrument have been observed by other investigators (Seelmann et al. 2019). CRM measurements from Cruises 1-5 showed clear, steady instrument drift of up to 93 µmol kg^{-1} by the end of Cruise 2, or a drift of nearly 3 µmol kg^{-1} per day (Supplementary Material Figure S2, Table S1). After the fifth cruise an inline cross-flow filter (0.2 µm) connected to a small 50 mL reservoir for filtered seawater was installed which eliminated the instrument drift during Cruises 6 and 7. The HydroFIA TA sample analysis time was 10 minutes, and flow rate supplied to the filter had to be adequate to replenish the reservoir within the analysis time frame. The cross-flow filter (currently supplied by 4H-JENA engineering GmbH, Jena, Germany, formerly Kongsberg Maritime Contros GmbH, Kiel, Germany) uses tangential flow filtration, where unfiltered seawater flowed continuously across the filter surface (in this case, a series of tubes of filter material) at

positive pressure, with filtrate moving through the walls of the tubes and collected in a reservoir for analysis. This method allowed the same filter to be used for all subsequent cruises.

To account for instrument drift over the first five cruises, the differences between the CRM TA concentration and the mean of periodic triplicate instrument CRM readings were linearly interpolated; the interpolated CRM difference corresponding to each individual TA measurement was then retrieved from the HydroFIA TA timestamp and subtracted from the observed reading.

Statistical Calculations

In order to evaluate the performance of the HydroFIA TA instrument and reference titration systems from two laboratories, several statistical quantities were calculated following the approach of Seelmann et al. (2019). Complete descriptions and equations are presented in the Supplementary Material. Briefly, five statistical parameters will be discussed. First, precision (σ) was determined as one standard deviation of repeated measurements of certified reference material (CRM). Second, instrument accuracy (or also the uncertainty between two measurement methods, such as HydroFIA TA and laboratory TA measurements) was determined as the root mean square error (*RMSE*) of either repeated CRM measurements relative to the certified CRM TA or the difference between paired TA analyses. Third, the uncertainty in instrument bias, *u(bias)*, incorporates the instrument *RMSE* and the known uncertainty of the certified TA of the CRM. Fourth, the combined method uncertainty, *uc*, incorporates *u(bias)* together with σ. Finally, the overall uncertainty between two TA measurement methods, such as HydroFIA TA and laboratory TA analyses, including factors such as replicate uncertainty and unknown uncertainties, is presented as $u_{c(HydroFIA\ TA,\ B)}$.

HydroFIA TA Analyzer and Discrete Sample Uncertainty Evaluation

Triplicate periodic CRM measurements were automatically made on a roughly daily interval by the HydroFIA TA while underway during each cruise, permitting an assessment of precision (σ, Equation 1). The CRM used in 2017 was Batch 159. For Cruises 1-5, the σ of triplicate CRM measurements ranged from ±0.2 to ±9.2 µmol kg^{-1}, with a mean σ of ±2.0 µmol kg^{-1}. Addition of the filter resulted in no substantial change in the σ of CRM measurements for Cruises 6 or 7 in 2017 (mean CRM σ ±0.8 and ±1.8 µmol kg^{-1}, respectively). Accuracy of the HydroFIA TA during Cruises 1 through 7 in 2017, determined as the RMSE of periodic CRM readings which were corrected as described above, ranged from ±1.0 to ±3.8 µmol kg^{-1} with a mean value of ±2.2 µmol kg^{-1}. These precision and accuracy levels matched or exceeded those given by the manufacturer (±2 and ±5 µmol kg^{-1}, respectively).

Discrete TA samples were collected on two cruises from the same underway seawater supply sampled by the HydroFIA TA (Table 2). AOML measurements of CRM Batches 129 and 144 resulted in an uncertainty (u_c) of ±2.8 µmol kg^{-1}. Analysis of duplicate seawater samples returned an AOML sampling uncertainty, u(rep), of ±5.2 µmol kg^{-1}. The RMSE of paired AOML-HydroFIA TA analyses was ±7.0; solving Equation 5 resulted in an estimated contribution of ±2.9 µmol kg^{-1} of 'other' uncertainty to the total uncertainty between AOML and HydroFIA TA measurements, beyond the combined uncertainties of instrument precisions, biases, CRM uncertainties, and sampling or replicate uncertainties.

The calculations described above were used to compare HydroFIA TA results to those measured onboard by U.Del. during the 2018 ECOA-2 cruise (Table 2). U.Del. analyses of CRM Batch 173 showed a low overall method uncertainty (u_c) of ±1.8 µmol kg^{-1} and very good agreement between replicate samples, with a u(rep) of ±0.9 µmol kg^{-1}. Despite an overall HydroFIA TA u_c similar to that from Cruise 1 in 2017 (±4.1 µmol kg^{-1}, from triplicate measurements of CRM Batch 173), the RMSE between HydroFIA TA and U.Del. measurements was a relatively high ±10.3 µmol kg^{-1}, with a u(other) of ±9.2 µmol kg^{-1}.

HydroFIA TA performance was consistent within ±2 µmol kg^{-1} across cruises, making it challenging to attribute the difference in u(other) between Cruise 1 in 2017 and ECOA-2. Possible factors contributing to u(other) could be the choice to preserve (AOML) or not preserve (U.Del.) discrete samples, the timing of discrete sample collection relative to the intake of sample by the HydroFIA TA, nonlinearity of the HydroFIA TA instrument drift as documented by Seelman et al. (2019), or variable effects of the presence of titratable organic species dependent on the TA analysis method used. It is important to note that organic species represent an unknown but potentially significant contributor to TA (Yang et al. 2015, Kuliński et al. 2014, Fong and Dickson 2019). Neither the HydroFIA TA analyzer nor typical discrete TA titrations are capable of distinguishing organic alkalinity contributions, which may exert a variable influence depending on the acid-base characteristics of the organic species and the TA analysis method employed (Sharp and Byrne, 2020). This topic requires further examination, but for this work we will discuss TA as the inorganic system conforming to the definition set by Dickson (1981).

Data Analysis

Linear regression analysis of salinity against TA was performed using an iteratively weighted least-squares algorithm with a bisquare weighting function (tuning constant 4.685) and robust fitting options enabled (*fitlm* in Matlab®, Mathworks, Natick MA USA). The robust fitting identified outliers as any point outside 1.5 times the interquartile above or below the 75th or 25th percentile, respectively, and outliers were excluded from the calculation of the r^2 statistic. This outlier analysis excluded outliers at roughly the 10th and 90th percentiles. The regression analysis returned two linear coefficients: the change in TA per unit salinity (i.e. slope, designated "TA:S" hereafter) and the TA calculated at salinity zero (i.e. intercept, designated "TA^0"). All regional and seasonal TA:S regressions were statistically unique according to one-way ANOVA tests, with p-values less than 0.05. Other studies (i.e. Lee et al.,

2006) used a second-order polynomial regression with both salinity and temperature as independent input variables, but this approach yielded worse RMSE statistics for our data (results not shown), and we have chosen to use the linear regression approach described above. Data were divided into seasons according to the following: winter (December, January, February), spring (March, April, May), summer (June, July, August), and fall (September, October, November).

Historical Data

To compare the results from this work to past observations in these regions, a historical dataset was assembled. Datasets used in this compilation included several categories: ship-of-opportunity measurements obtained from NOAA's AOML, data from the GOMECC-1 and -2 and ECOA-1 East Coast surveys, newly-available data from Fisheries and Oceans, Canada (DFO), the global-scale GLODAPv2 (2019) synthesis product, and data from the Ocean Margins Project (OMP) in the MAB. The earliest TA observations made in the four study regions discussed in this work were from 1967, with the number of observations increasing steadily to the present, and with occasional years-long periods having no observations. The dataset contains over 11,000 surface measurements at depths of 10 m or less.

Results and Discussion

HydroFIA TA measurements were collected on seven *Bigelow* cruises between February 11, 2017 and July 19, 2017 (Figure 2), resulting in a total of 8,950 surface seawater TA measurements (Table 1) and 167 CRM validation measurements. The same HydroFIA TA instrument used in 2017 aboard the *Bigelow* was also deployed during the 2018 ECOA-2 cruise, for 28 days in July and August 2018, collecting a total of 1,656 TA and 75 CRM validation measurements. The 2018 ECOA-2 cruise occupied

the same regions as the 2017 cruises (Figure 2) and included a much more spatially comprehensive survey of the SAB region. To exploit the large number of new measurements made by the HydroFIA TA instrument, we examine the data obtained during the deployments aboard the *Bigelow* in the context of previously published analyses of TA distributions, and use these new observations to examine published relationships relating TA to sea surface salinity. We also re-evaluate data from other broad-scale data collections efforts in these regions. These comparisons are not meant to show that one dataset provides a better or worse understanding of TA conditions relative to another; rather, they are meant to show that TA conditions are dynamic in these coastal zones, and the capability provided by the largely unsupervised deployment of the HydroFIA TA system can help fill in knowledge gaps regarding seasonal and regional dynamics in ways that episodic research cruises collecting a necessarily limited number of discrete water samples cannot.

Salinity, water temperature, and TA generally increased from north to south in 2017, as upstream Scotian Shelf water feeds a coastal current flowing southward through the GOM and GBN regions to the MAB region, while gradually being modified by interactions with local rivers and offshore SBF water masses (Figures 3 and 4, Table 3). Salinity and TA were lowest closer to shore and increased with distance from the coast in the GOM, GBN and MAB regions. The SBF region extends seaward from the outer boundary of each of the other regions, and was generally warmer, saltier, and higher in TA than the more shoreward regions. The SBF region contains a combination of slope water modified by interaction with the southward-flowing coastal shelf water along the boundary lines between the MAB, GBN and GOM regions (Dupont et al. 2006).

The increasing north-to-south trend in salinity, water temperature and TA was generally repeated in 2018, but the MAB region was an exception to this trend, as the MAB mean salinity (31.19±1.07) and TA (2132±43 µmol kg^{-1}) were both lowest among the studied regions. The ECOA-2 cruise made a shore stop in the MAB region, and the low-salinity data recorded outside the Newport

News harbor mouth contributed to the low mean values (Xu et al. 2017). Nonetheless, even when these nearshore data are excluded the mean salinity and TA were still the lowest among the regions.

In contrast, seawater pCO_2 showed no clear regional pattern, and was almost always undersaturated or at near equilibrium with respect to the atmospheric CO_2 partial pressure (Table 3). Atmospheric pCO_2 measured by the shipboard AOML system averaged 412±6 µatm. To test for significant differences among regional observations, we employed two-sample t-tests ('ttest2' in Matlab®, Mathworks Inc., Natick MA, USA), at a significance level (p) of 0.01. These tests showed that mean salinity, sea surface temperature, pCO_2 and TA were all statistically different between all regions in the 2017 dataset (Table 3). These differences are attributed to circulation patterns, variability of contributions from upstream or offshore water masses, terrestrial inputs, or biogeochemical processes; likely the variability is due to a combination of all those factors. The same t-tests indicated that salinity, water temperature, TA and pCO_2 were all significantly different amongst the regions during ECOA-2.

Regional Salinity:TA Regressions

Regressions of regional HydroFIA TA data against salinity showed clear differences between years, regions, and seasons (Figures 6-9). Broadly, the slope of the TA:S regression line for all 2017 data increased from the GOM (24.9±0.3) to GBN (36.6±0.6) to MAB (36.7±0.3) regions along the path of southward-flowing coastal water, while TA^0 decreased from north to south (1395±8, 1011±19, and 1008±11 µmol kg^{-1}, respectively). This pattern of increasing slope and decreasing TA^0 from north-to-south is consistent with the results of Cai et al. (2010), but the TA:S regression coefficients were distinctly different from those found by Cai et al. (2010) for all regions, with uniformly shallower slopes and higher TA^0. The 2018 ECOA-2 data showed an opposite pattern to that from 2017, with decreasing TA:S slope from the GOM to GBN to MAB regions (62.7, 52.5, 38.5, respectively) and increasing TA^0 (178,

497, 936 µmol kg^{-1}, respectively). The regressions of surface TA against salinity were again distinctly different from those found by Cai et al. (2010) for all regions, with uniformly shallower slopes and higher TA^0 (Figure 10), although the GOM slope (62.7) and intercept (178 µmol kg^{-1}) for 2018 were somewhat similar to the low-salinity GOM slope (65.8) and TA^0 (75.1 µmol kg^{-1}) from Cai et al. (2010). It is important to mention here that the TA-salinity relationships presented in Cai et al. (2010) were constructed from data acquired throughout the water column, from the surface to deeper slope and shelf waters, with the deepest samples ranging from 200-290 m. Thus, direct comparison between the surface measurements presented in this work and the deeper measurements used by Cai et al. (2010) may be unrealistic as contributions from various water masses are likely unequal.

Seasonal TA:S shifts were found in the GOM (Figure 6). The 2017 winter TA:S slope (41.3) and TA^0 (852 µmol kg^{-1}) were similar to the high-salinity values of Cai et al. (2010, data collected in summer), who reported a slope and TA^0 of 39.1 and 932 µmol kg^{-1}, but during the springtime in 2017 (March through May) the GOM TA:S changed substantially, with a much shallower slope (24.3), higher TA^0 (1415 µmol kg^{-1}), and lower r^2 (0.77). These conditions persisted into the summer of 2017 (June and July) in the GOM, and contrast sharply with the GOM TA:S regression in the summer of 2018. A similar 2017 seasonal shift was seen in the GBN region (Figure 7) from winter, through spring and into summer, with progressively shallower slopes (32.3, 30.2, and 18.4, respectively), higher TA^0 (1160, 1215, 1600, respectively), and lower r^2 (0.63, 0.63, 0.40, respectively).

Seasonal regressions from the MAB region in 2017 were lagged in time compared to those from the GOM and GBN regions. MAB winter and spring 2017 TA:S results were quite consistent in 2017 (Figure 8), with similar TA:S slopes (40.8 and 44.1, respectively) and TA^0 (880 and 763 µmol kg^{-1}, respectively), and encompassed the MAB slope and TA^0 provided by the historical dataset (43.7 and 769 µmol kg^{-1}, respectively). The summer MAB regression changed substantially in a similar fashion to the

GOM and GBN regions, with the TA:S slope dropping from 44.1 to 14.5 and TA^0 increasing from 763 to 1726 µmol kg^{-1}.

SBF TA:S regressions further reinforce the observation that a seasonal shift occurred, as SBF winter and spring slope (44.2 and 42.2, respectively) and TA^0 (761 and 821 µmol kg^{-1}, respectively) were similar in 2017, whereas the summer slope (21.7) and TA^0 (1497 µmol kg^{-1}) were markedly different (Figure 9). SBF results are also notably differentiated by latitude: Steeper SBF winter and spring slopes were influenced by data from latitudes at or below 39°N, whereas the shallower summer SBF slope was mostly controlled by data from latitudes higher than 40°N. Cruise tracks from 2017 (Figure 2) showed that the SBF data north of 40°N were collected in a region near the confluence of the SBF, GOM, and MAB regions, whereas the cruise tracks south of 39°N ran very close to the boundaries between the SBF and MAB regions. The SBF slope from 2018 (46.9) was similar to the steeper, lower-latitude 2017 data group and the historical SBF slope (47.9). The 2018 SBF data also followed a uniform linear trend regardless of latitude.

The work of Lee et al. (2006) presented a polynomial expression of both salinity and sea surface temperature for the estimation of TA in North Atlantic surface waters, so direct comparison of linear regression coefficients is not possible here. The GOM equation of Cai et al. (2010) returned TA closer to measured values in 2017 (mean difference 8±14 µmol kg^{-1}, Table 4) compared to the Lee et al. (2006) equation including in situ sea surface temperature (mean difference 13±10 µmol kg^{-1}). The reverse was true in the MAB region where the TA calculated according to Lee et al. (2006) was more similar to the observed HydroFIA TA values (mean difference 1±12 µmol kg^{-1}) than TA calculated from the Cai et al. (2010) equation (mean difference 12±16 µmol kg^{-1}). The GBN region was represented equally well in 2017 by the Lee et al. (2006) equation (mean difference 4±10 µmol kg^{-1}) and Cai et al. (2010) equation (mean difference -5±16 µmol kg^{-1}).

Regional and seasonal changes in TA:S combine to form a cohesive trend in 2017. During winter, the TA:S slope and TA^0 for all regions except the SBF were indistinguishable both from those of Cai et al. (2010, Figures 6-9) and from historical TA:S trends (Figure 10). The winter SBF slope (44.2), while not indistinguishable, still resembled the slope from the historical dataset (47.9) as well as the "Atlantic" slope of 51.2 presented by Millero et al. (1998, Figure 9). Thus, the winter of 2017 data appear to reflect 'typical' conditions consistent with previous findings. In contrast, atypical conditions developed in the GOM in the spring of 2017 and continued into the summer and expanded southward and westward to the GBN, MAB, and SBF regions. By the summer of 2017, all regions showed TA:S conditions quite different from both the historical dataset and the results of Cai et al. (2010). These atypical summer conditions were not reflected in the 2018 ECOA-2 data, so the progression seen in 2017 is likely not due to typical seasonal patterns. Instead, the historical data show that the shifts in 2017 were opposite of the typical seasonal changes in TA:S slope and TA^0.

Seasonal Biases in Data Availability

It is important to note here the paucity of available historical TA observations in winter; despite collecting the broadest extent of data we could find, there were no surface TA measurements in any region in January, and only about 25 GOM measurements in December (Figure 5). The vast majority of historical winter measurements were taken in February, and the existing East Coast TA data are overall heavily weighted towards summertime sampling. Data collected aboard the *Bigelow* in 2017 by the HydroFIA TA instrument provided some of the first widely spatially-distributed TA measurements along the East Coast outside the summer months, as the GOMECC and ECOA cruises were all conducted during the summer months of June, July and August. Regular NOAA Ecosystem Monitoring (EcoMon) cruises have been conducted since 2012 during non-summer months, including TA sampling, but with a limited

number of stations. Incorporation of the data collected in this work increases available TA observations by more than one order of magnitude during the months when the HydroFIA TA system was deployed. Winter is a difficult time to conduct cruises in Atlantic waters, but it is also a biologically important season, as it sets up conditions for the springtime bloom. The lack of historical evidence of shifts in seasonal TA:S, such as we have shown, may not be because these shifts are rare, but because the data have not been available to detect them.

Mechanisms Affecting Linear TA:S Relationships

A variety of processes can alter ocean TA and salinity, contribute to TA:S variability, and potentially contribute to the observations presented here. Over time scales greater than 100,000 years, alkalinity (and salinity) in the oceans are controlled by geologic weathering and net seafloor sedimentary processes whereas over time scales between 1,000 and 100,000 years surface alkalinity is controlled by variations in biological pumping and interactions with carbonate and silici-clastic sediments (Zeebe 2012). On shorter time scales, Takahashi et al. (2014) described five "oceanographic situations" and their effect upon the linear TA:S relationship. These situations, which will be discussed in terms of their applicability to the findings from this study, are: (a) evaporation-precipitation (b) mixing in subtropical gyres between subtropical waters (whose TA is depleted by calcareous organism growth) and fresher subpolar waters enhanced in TA due to upwelling (c) biological production and decomposition, especially of $CaCO_3$-containing shells (d) mixing of a source water with river water containing higher or lower TA, and (e) mixing of a source water with another body of water containing higher salinity and reduced TA (such as a warm evaporative basin or upwelled slope waters). As evaporation-precipitation (a) alters salinity and TA in proportion, this process will not affect the TA:S relationship. Neighboring regions exhibiting higher salinity and TA include the coastal SAB region to the south and the more

offshore Gulf Stream water mass, providing two possible sources contributing to process (e). The regions in this study are likely not large enough to reflect changes in subtropical-subpolar mixing over seasonal time scales (e.g. Fry et al. 2015), and thus process (b) can be discounted. This leaves the situations of biological production (c), river water mixing (d), or mixing with a higher salinity water mass (e) as the most likely processes affecting the TA:S relationships in these regions.

The Effect of Net Calcification or Dissolution

$CaCO_3$ production events have been shown to lower TA (Bates et al. 1996a, Bates 2001), and therefore alter the slope of the TA:S line. In a regional context, uniform production across the region would result in no change to the TA:S line, whereas higher production in the saltier waters of a region would lead to a decreased TA:S slope, and higher production in the lower salinity waters would lead to an increased slope. This biological utilization in high-nutrient waters can potentially account for up to a 50 µmol kg^{-1} TA reduction (Takahashi et al. 2014, Bates et al. 1996b, Harlay et al. 2010). It is conceivable that an offshore bloom of a calcifying species (such as a coccolithophore) could have drawn down TA in 2017, reducing the slope of the TA:S mixing line. This could explain the high-salinity data in 2017 that fall well below the Millero et al. (1998) regression line (Figure 9), but corresponding $CaCO_3$ dissolution is needed to explain the low-salinity data that fall above the Millero et al. (1998) line. This can be seen especially in the offshore SBF region, where the 2017 summertime TA:S line appears to be rotated about a salinity of 33 relative to the other SBF regression lines, with lower TA above salinity 33 and higher TA below (Figure 9). An offshore calcifying bloom could explain the apparent TA drawdown above salinity 33, with corresponding $CaCO_3$ dissolution inshore explaining the elevated TA input below salinity 33. Indeed, reductions in the TA:S slopes in the GOM, GBN and MAB regions all appear to be due to lower-salinity TA enhancement (Figures 6-8).

The formation of $CaCO_3$ by calcifying species results in elevated pCO_2 through shifts in the DIC:TA ratio, with the opposite effect for $CaCO_3$ dissolution (Zeebe 2012, Bates et al. 1996b); however, the overall net pCO_2 change depends on the amount of $CaCO_3$ formation or dissolution relative to net ecosystem production. Thus, elevated pCO_2 levels would be expected in areas where calcification is the primary mechanism of TA:S variability, and reduced pCO_2 in those areas where dissolution predominates, although other mechanisms may offset some or all of this pCO_2 increase (Balch 2018). In the case of the GOM region, the mean 2017 summer pCO_2 (335 µatm) was lower than any other sampling period within the GOM region for this study, a potential indication of $CaCO_3$ dissolution, or alternatively high net productivity. For a historical climatological comparison all surface pCO_2 measurements within each study region were extracted for each season from the 2019 Surface Ocean CO_2 Atlas with data from 1957 to 2019 (SOCAT2019, Bakker et al. 2016). The mean GOM pCO_2 in summer 2017 (336 µatm) was significantly lower than the historical (2002-2018) mean GOM summer pCO_2 from the SOCAT database (370 µatm) as well as the mean GOM pCO_2 from the 2018 ECOA-2 cruise (390 µatm, significance determined according to one-way ANOVA tests, see Supplementary Material Figure S3). Some of this difference may be due to the colder temperature in 2017 resulting in lower pCO_2. Furthermore, the 2017 summer MAB and SBF mean pCO_2 values (376 and 366 µatm, respectively) were significantly lower than the respective values from summer 2018 during the ECOA-2 cruise (421 and 398 µatm, respectively) or seasonal mean pCO_2 from the SOCAT database (411 and 392 µatm, respectively). While the presence of lower pCO_2 concurrent in space and time with the atypical TA:S relationships supports the idea that $CaCO_3$ dissolution resulted in elevated TA:S slopes in the coastal GOM and MAB regions, this mechanism is unlikely given that these surface waters are typically supersaturated with $CaCO_3$ (Wanninkhof et al. 2015).

Potential River or Shelf Mixing Effects

Mechanisms (d), mixing of a source water with river water containing higher or lower TA and (e), mixing with a higher salinity water mass, remain as explanations to the observed seasonal TA:S shifts. Cai et al. (2010) characterized the GOM, GBN and MAB regions as “Current-Dominated Margins”, where freshwater and TA inputs from local rivers are greatly outweighed by those carried by alongshore currents. For regions in this study, the dominant alongshore current is the southward-flowing Labrador Current, a branch of which travels successively southward through the GOM, GBN, and MAB regions. Recent rapid warming of the Gulf of Maine (Pershing et al. 2015, Pershing et al. 2018) has been linked to increased intrusions of deeper, salty, and warm water through the Northeast Channel and concurrent reductions in Labrador water (Figure 1, Townsend et al. 2015, Brickman et al. 2018), the prevalence of which are in turn affected by changes in the Atlantic Meridional Overturning Circulation (Sherwood et al. 2011, Claret et al. 2018) or changes in the strength of the Labrador Current inflows (Jutras et al. 2020). Cai et al. (2010) suggest that continuous mixing of regional surface water with deeper slope and shelf waters would result in the lowering of the TA:S slope, providing a possible explanation of the seasonal shifts seen in this study. This explanation may not be satisfactory, as the regional salinities in 2017 generally decreased from winter to spring and then summer, while the TA at lower salinity gradually rises above the mixing line, suggesting a change in the amount of freshwater and TA being carried into the region.

The seasonal TA:S shifts seen in the 2017 data may have resulted from an increase of upstream shelf water entering the GOM relative to warm slope water. GOM temperature anomaly analyses, updated through 2020 using methods described by Pershing et al. (2015), show that GOM surface temperatures in early 2017 (January and February) were high enough to be judged a ‘heat wave’ (Pershing et al. 2018, updated data presented at https://www.gmri.org/stories/gulf-maine-temperature-update-normal-new-cold/, accessed 10/4/2020). The GOM surface water temperature then fell through the spring and early summer to either lower-than-usual or typical values, indicating a transition from

warmer, saltier source water to colder, fresher shelf water. Cai et al. (2010) report a Labrador TA:S regression slope of 33 and TA^0 of 1124 µmol kg^{-1}. These values are lower than the 2017 summer GOM slope and TA^0 in this study (26.2 and 1357 µmol kg^{-1}, respectively, Figure 10). As the Labrador Current travels from the Labrador Sea to our study regions and becomes shelf water, it is modified by other inputs, notably those from the St. Lawrence Estuary, which carries massive amounts of freshwater to the Atlantic coast north of Nova Scotia. St. Lawrence Estuary TA^0 (1124-1314 µmol kg^{-1}, Dinauer and Mucci 2017, 2018) is typically lower than the TA^0 calculated for spring 2017 in the GOM (1415 µmol kg^{-1}) and summer 2017 in all study regions- all TA^0 values which statistically exceed the historical TA^0 for each region by wide margins. Whereas the St. Lawrence experienced a large flooding event in early 2017 (ILO-SLRB 2018), the water transit time of more than six months between the St. Lawrence and the Gulf of Maine discounts the influence of the St. Lawrence on our 2017 observations (Ohashi and Sheng 2013). Measured TA^0 values from local rivers in the GOM, GBN, and MAB regions (Hunt et al. 2011, Cai et al. 2010) are much too low to account for the elevated TA^0 measured in this study, and discharge levels from these rivers are too small to broadly impact the biogeochemistry of these regions (Cai et al. 2010).

We compared surface salinity measured in this study to climatological data from the World Ocean Atlas 2018 (WOA2018) salinity product (Zweng et al. 2019). Gridded monthly North Atlantic and Coastal WOA2018 salinity at 1/4° resolution was retrieved, and the same regional boundaries discussed previously were used to compute seasonal, climatological statistics for the GOM, GBN, MAB and SBF regions. In three of the four study regions (GOM, GBN, and SBF), the 2017 mean summer salinity was lower than that from winter or spring 2017, and lower than the seasonal mean WOA salinity for winter, spring or summer (see Supplementary Material Figure S3). The GBN and SBF 2017 mean summer salinities were also lower than those from ECOA-2. The one exception is the MAB region, where the mean 2017 summer salinity was indistinguishable from the mean summer salinity during ECOA-2 or from the WOA, and all were lower than the 2017 mean winter and spring salinities. These exceptionally

low salinities show the abnormal levels of freshwater present in the regions, which cannot be accounted for by local river discharge, and instead must be transported southward by upstream sources.

Mixing with freshwater can potentially explain the 2017 changes in TA:S slope but cannot readily explain the relatively low TA at salinities greater than 35, which were observed around Cape Hatteras. Lower than usual pCO_2 suggests that biological uptake through calcification was not likely, and thus another high-salinity endmember, with characteristic TA much lower than the Gulf Stream is needed. One possibility is provided by Cai et al. (2010), who describe TA:S regressions from seven South Atlantic Bight (SAB) shelf cruises resulting in a calculated TA at salinity 36.5 of 2386-2400 µmol kg^{-1}, with a mean value of 2384 µmol kg^{-1}. The same paper lists an unusual TA:S slope and TA^0 from a series of GYRE93 cruises around the intersection of the MAB and SAB regions which result in an unusually low calculated TA at salinity 36.5 of 2300 µmol kg^{-1}, and support the concept that the observed 2017 TA from this study at salinity 36.5 (2355 µmol kg^{-1}) is low but not unprecedented. The SAB thus represents a potential high-salinity/low TA water source, through surface water exchange between coastal SAB waters inshore of the Gulf Stream and the MAB and SBF regions, or SBF water transported northwards via the Gulf Stream and then eastwards into the MAB region via eddies or warm-core rings (Rasmussen et al. 2005, Hare and Cowen 1996).

Previous work has discussed a mean southward flow of coastal water from the GOM, through the GBN, and into the MAB region (Townsend et al. 2006, Cai et al. 2010, Wang et al. 2013, Wanninkhof et al. 2015), with both salinity and TA enriched by mixing with slope waters along the way. The measurements made as part of this study, as well as the historical data discussed above, indicate that the surface water conditions are substantially more complex between regions and across seasons. In addition to the alongshore gradient in TA, there also appears to be an offshore influence as well, as warmer and saltier north-flowing Gulf Stream water interacts with southward-flowing coastal water masses. The mixing balance between the saltier, TA-enriched northward-flowing Gulf Stream water, the

southward-flowing shelf water, and deeper slope water may dictate much of the distribution of salinity and TA along the East Coast.

Conclusions

Deployment of the CONTROS HydroFIA® TA instrument aboard the *Bigelow* produced high quality (u_c of 2.4-4.1 µmol kg^{-1}) surface TA data over broad spatial and temporal time scales. Results from 2017 and 2018 showed that use of the HydroFIA TA instrument aboard cruises of opportunity can greatly increase regional carbonate system monitoring capacity. Linear annual and seasonal comparisons showed that TA distributions along the United States East Coast are dynamic, not easily predicted from physical variables such as salinity, and not yet fully characterized by current studies. Significant seasonal shifts in linear TA:S relationships demonstrate potential problems with any single linear model for the retrieval of TA from salinity. Analysis of a compiled historical regional dataset reinforces the finding that salinity, TA, and TA:S linear relationships shift seasonally, although data availability is extremely sparse in some months and regions. Additional deployments during undersampled months may further advance the understanding of the seasonal nature of TA:S relationship in these regions, and analyses of derived DIC, pH or carbonate saturation state may provide even more insights. Especially when deployed on ships equipped with instrumentation to measure another carbonate system parameter (i.e. pCO_2), the HydroFIA TA instrument represents a substantial advancement in the ability to comprehensively monitor and characterize surface waters.

Acknowledgements

This work was supported by NOAA TTP Project NA15NOS0120155- Tracking Ocean Alkalinity using New Carbon Measurement Technologies (TAACT). The comments provided by three reviewers and Associate Editor A. Mucci were invaluable in improving this work. We gratefully acknowledge the extensive shipboard and laboratory assistance of Christopher Taylor, Mark Bradley, Marc Emond, Katherine McGinnis, and Shawn Shellito, Denis Pierrot of AOML for providing pCO_2 data, and the incomparable support provided by Jacob Sobin of Kongsberg Underwater Technology, LLC.

References

Aßmann, S., Frank, C., Petersen, W., Körtzinger, A., 2013. Autonomous pH and alkalinity sensors for the characterization of the carbonate system in coastal areas. Presented at the EGU General Assembly Conference Abstracts, pp. EGU2013-8760.

AOML. HB1701 Cruise Report. Accessed September 25, 2020. https://www.aoml.noaa.gov/ocd/gcc/shortcruises/HB1701/33HH20170210-HB1701-Readme.pdf.

Bakker, D.C.E., Pfeil, B., Landa, C.S., Metzl, N., O'Brien, K.M., Olsen, A., Smith, K., Cosca, C., Harasawa, S., Jones, S.D., Nakaoka, S., Nojiri, Y., Schuster, U., Steinhoff, T., Sweeney, C., Takahashi, T., Tilbrook, B., Wada, C., Wanninkhof, R., Alin, S.R., Balestrini, C.F., Barbero, L., Bates, N.R., Bianchi, A.A., Bonou, F., Boutin, J., Bozec, Y., Burger, E.F., Cai, W.-J., Castle, R.D., Chen, L., Chierici, M., Currie, K., Evans, W., Featherstone, C., Feely, R.A., Fransson, A., Goyet, C., Greenwood, N., Gregor, L., Hankin, S., Hardman-Mountford, N.J., Harlay, J., Hauck, J., Hoppema, M., Humphreys, M.P., Hunt, C.W., Huss, B., Ibánhez, J.S.P., Johannessen, T., Keeling, R., Kitidis, V., Körtzinger, A., Kozyr, A., Krasakopoulou, E., Kuwata, A., Landschützer, P., Lauvset, S.K., Lefèvre, N., Monaco, C.L., Manke, A., Mathis, J.T., Merlivat, L., Millero, F.J., Monteiro, P.M.S., Munro, D.R., Murata, A., Newberger, T., Omar, A.M., Ono, T., Paterson, K., Pearce, D., Pierrot, D., Robbins, L.L., Saito, S., Salisbury, J., Schlitzer, R., Schneider, B., Schweitzer, R., Sieger, R., Skjelvan, I., Sullivan, K.F., Sutherland, S.C., Sutton, A.J., Tadokoro, K., Telszewski, M., Tuma, M., Heuven,

S.M.A.C. van, Vandemark, D., Ward, B., Watson, A.J., Xu, S., 2016. A multi-decade record of high-quality fCO2 data in version 3 of the Surface Ocean CO2 Atlas (SOCAT). Earth System Science Data 8, 383–413. https://doi.org/10.5194/essd-8-383-2016Balch, W. M. 2018. The Ecology, Biogeochemistry, and Optical Properties of Coccolithophores. Annual Review of Marine Science 10: 71–98. doi:10.1146/annurev-marine-121916-063319.

Balch, W. M. 2018. The Ecology, Biogeochemistry, and Optical Properties of Coccolithophores. Annual Review of Marine Science 10: 71–98. doi:10.1146/annurev-marine-121916-063319.

Barbero, L., D. Pierrot, R. Wanninkhof, and others. 2017. Third Gulf of Mexico Ecosystems and Carbon Cycle (GOMECC-3) Cruise. Cruise Report. doi :10.25923/y6m9-r,08

Bates, N.R., Michaels, A.F., Knap, A.H., 1996a. Seasonal and interannual variability of oceanic carbon dioxide species at the U.S. JGOFS Bermuda Atlantic Time-series Study (BATS) site. Deep Sea Research Part II: Topical Studies in Oceanography 43, 347–383. https://doi.org/10.1016/0967-0645(95)00093-3

Bates, N.R., Michaels, A.F., Knap, A.H., 1996b. Alkalinity changes in the Sargasso Sea: geochemical evidence of calcification? Marine Chemistry 51, 347–358. https://doi.org/10.1016/0304-4203(95)00068-2

Bates, N.R., 2001. Interannual variability of oceanic CO2 and biogeochemical properties in the Western North Atlantic subtropical gyre. Deep Sea Research Part II: Topical Studies in Oceanography 48, 1507–1528. https://doi.org/10.1016/S0967-0645(00)00151-X

Breitburg, D.L., Salisbury, J., Bernhard, J.M., Cai, W.-J., Dupont, S., Doney, S.C., Kroeker, K.J., Levin, L.A., Long, W.C., Milke, L.M., Miller, S.H., Phelan, B., Passow, U., Seibel, B.A., Todgham, A.E., Tarrant, A.M., 2015. And on Top of All That…: Coping with Ocean Acidification in the Midst of Many Stressors. Oceanography 28, 48–61.

Brickman, D., D. Hebert, and Z. Wang. 2018. Mechanism for the recent ocean warming events on the Scotian Shelf of eastern Canada. Continental Shelf Research 156: 11–22. doi:10.1016/j.csr.2018.01.001.

Cai, W.-J., Hu, X., Huang, W.-J., Jiang, L.-Q., Wang, Y., Peng, T.-H., Zhang, X., 2010. Alkalinity distribution in the western North Atlantic Ocean margins. J. Geophys. Res. 115, C08014. https://doi.org/10.1029/2009JC005482

Cai, W.-J., X. Hu, W.-J. Huang, and others. 2011. Acidification of subsurface coastal waters enhanced by eutrophication. Nature Geosci 4: 766–770. doi:10.1038/ngeo1297

Chen, C.-T.A., Wang, S.-L., 1999. Carbon, alkalinity and nutrient budgets on the East China Sea continental shelf. Journal of Geophysical Research: Oceans 104, 20675–20686. https://doi.org/10.1029/1999JC900055

Chipman, D.W., Sutherland, S.C., Takahashi, T., 1995. Determination of ocean/atmosphere carbon dioxide flux within the OMP study area. Final Technical Report for Grant DE-FG02-92ER61451, Lamont–Doherty Observatory of Columbia University, 16 pp.

Claret, M., E. D. Galbraith, J. B. Palter, D. Bianchi, K. Fennel, D. Gilbert, and J. P. Dunne. 2018. Rapid coastal deoxygenation due to ocean circulation shift in the northwest Atlantic. Nature Climate Change 8: 868–872. doi:10.1038/s41558-018-0263-1.

Cross, J.N., Mathis, J.T., Bates, N.R., Byrne, R.H., 2013. Conservative and non-conservative variations of total alkalinity on the southeastern Bering Sea shelf. Marine Chemistry 154, 100–112. https://doi.org/10.1016/j.marchem.2013.05.012

DeGrandpre, M.D., Hammar, T.R., Wallace, D.W.R., Wirick, C.D., 1997. Simultaneous mooring-based measurements of seawater CO2 and O2 off Cape Hatteras, North Carolina. Limnology and Oceanography 42, 21–28. https://doi.org/10.4319/lo.1997.42.1.0021

DeGrandpre, M.D., Olbu, G.J., Beatty, C.M., Hammar, T.R., 2002. Air–sea CO2 fluxes on the US Middle Atlantic Bight. Deep Sea Research Part II: Topical Studies in Oceanography, Carbon Cycling and Biogeochemistry in the Northwest Atlantic Shel f Slope: Results of the Ocean Margins Program 49, 4355–4367. https://doi.org/10.1016/S0967-0645(02)00122-4

Dickson, A.G., 1981. An exact definition of total alkalinity and a procedure for the estimation of alkalinity and total inorganic carbon from titration data. Deep Sea Research Part A. Oceanographic Research Papers 28, 609–623. https://doi.org/10.1016/0198-0149(81)90121-7

Dickson, A.G., Afghan, J.D., Anderson, G.C., 2003. Reference materials for oceanic CO2 analysis: a method for the certification of total alkalinity. Marine Chemistry 80, 185–197. https://doi.org/10.1016/S0304-4203(02)00133-0

Dickson, A.G., Sabine, C.L. and Christian, J.R. (Eds.), 2007. Guide to Best Practices for Ocean CO2 Measurements. PICES Special Publication 3, 191 pp.

Dinauer, A., and A. Mucci. 2017. Spatial variability in surface-water pCO2 and gas exchange in the world's largest semi-enclosed estuarine system: St. Lawrence Estuary (Canada). Biogeosciences 14: 3221–3237. doi:https://doi.org/10.5194/bg-14-3221-2017

Dinauer, A., and A. Mucci. 2018. Distinguishing between physical and biological controls on the spatial variability of pCO2: A novel approach using OMP water mass analysis (St. Lawrence, Canada),. Marine Chemistry 204: 107–120.

Doney, S.C., Ruckelshaus, M., Emmett Duffy, J., Barry, J.P., Chan, F., English, C.A., Galindo, H.M., Grebmeier, J.M., Hollowed, A.B., Knowlton, N., Polovina, J., Rabalais, N.N., Sydeman, W.J., Talley, L.D., 2011. Climate Change Impacts on Marine Ecosystems. Annu. Rev. Mar. Sci. 4, 11–37. https://doi.org/10.1146/annurev-marine-041911-111611

Dupont, F., Hannah, C.G., Wright, D.G., 2006. Model investigation of the Slope Water, north of the Gulf Stream. Geophysical Research Letters 33. https://doi.org/10.1029/2005GL025321

Feely, R.A., Sabine, C.L., Lee, K., Berelson, W., Kleypas, J., Fabry, V.J., Millero, F.J., 2004. Impact of Anthropogenic CO2 on the CaCO3 System in the Oceans. Science 305, 362–366. https://doi.org/10.1126/science.1097329

Fine, R.A., Willey, D.A., Millero, F.J., 2017. Global variability and changes in ocean total alkalinity from Aquarius satellite data. Geophysical Research Letters 44, 261–267. https://doi.org/10.1002/2016GL071712

Fong, M.B., Dickson, A.G., 2019. Insights from GO-SHIP hydrography data into the thermodynamic consistency of CO2 system measurements in seawater. Marine Chemistry 211, 52–63. https://doi.org/10.1016/j.marchem.2019.03.006

Friedlingstein, P., Jones, M.W., O'Sullivan, M., Andrew, R.M., Hauck, J., Peters, G.P., Peters, W., Pongratz, J., Sitch, S., Quéré, C.L., Bakker, D.C.E., Canadell, J.G., Ciais, P., Jackson, R.B., Anthoni, P., Barbero, L., Bastos, A., Bastrikov, V., Becker, M., Bopp, L., Buitenhuis, E., Chandra, N., Chevallier, F., Chini, L.P., Currie, K.I., Feely, R.A., Gehlen, M., Gilfillan, D., Gkritzalis, T., Goll, D.S., Gruber, N., Gutekunst, S., Harris, I., Haverd, V., Houghton, R.A., Hurtt, G., Ilyina, T., Jain, A.K., Joetzjer, E., Kaplan, J.O., Kato, E., Klein Goldewijk, K., Korsbakken, J.I., Landschützer, P., Lauvset, S.K., Lefèvre, N., Lenton, A., Lienert, S., Lombardozzi, D., Marland, G., McGuire, P.C., Melton, J.R., Metzl, N., Munro, D.R., Nabel, J.E.M.S., Nakaoka, S.-I., Neill, C., Omar, A.M., Ono, T., Peregon, A., Pierrot, D., Poulter, B., Rehder, G., Resplandy, L., Robertson, E., Rödenbeck, C., Séférian, R., Schwinger, J., Smith, N., Tans, P.P., Tian, H., Tilbrook, B., Tubiello, F.N., Werf, G.R. van der, Wiltshire, A.J., Zaehle, S., 2019. Global Carbon Budget 2019. Earth System Science Data 11, 1783–1838. https://doi.org/10.5194/essd-11-1783-2019

Fry, C.H., Tyrrell, T., Hain, M.P., Bates, N.R., Achterberg, E.P., 2015. Analysis of global surface ocean alkalinity to determine controlling processes. Marine Chemistry 174, 46–57. https://doi.org/10.1016/j.marchem.2015.05.003

Gran, G. 1952. Determination of the equivalence point in potentiometric titrations. Part II. Analyst 77: 661–671. doi:10.1039/AN9527700661

Grodsky, S.A., Vandemark, D., Feng, H., Levin, J., 2018. Satellite detection of an unusual intrusion of salty slope water into a marginal sea: Using SMAP to monitor Gulf of Maine inflows. Remote Sensing of Environment 217, 550–561. https://doi.org/10.1016/j.rse.2018.09.004

Hagens, M., Slomp, C.P., Meysman, F.J.R., Seitaj, D., Harlay, J., Borges, A.V., Middelburg, J.J., 2015. Biogeochemical processes and buffering capacity concurrently affect acidification in a seasonally hypoxic coastal marine basin. Biogeosciences 12, 1561–1583. https://doi.org/10.5194/bg-12-1561-2015

Hare, J.A., Cowen, R.K., 1996. Transport mechanisms of larval and pelagic juvenile bluefish (Pomatomus saltatrix) from South Atlantic Bight spawning grounds to Middle Atlantic Bight nursery habitats. Limnology and Oceanography 41, 1264–1280. https://doi.org/10.4319/lo.1996.41.6.1264

Harlay, J., Borges, A.V., Van Der Zee, C., Delille, B., Godoi, R.H.M., Schiettecatte, L.-S., Roevros, N., Aerts, K., Lapernat, P.-E., Rebreanu, L., Groom, S., Daro, M.-H., Van Grieken, R., Chou, L., 2010. Biogeochemical study of a coccolithophore bloom in the northern Bay of Biscay (NE Atlantic Ocean) in June 2004. Progress in Oceanography 86, 317–336. https://doi.org/10.1016/j.pocean.2010.04.029

Hofmann, E., Druon, J.-N., Fennel, K., Friedrichs, M., Haidvogel, D., Lee, C., Mannino, A., McClain, C., Najjar, R., O'Reilly, J., Pollard, D., Previdi, M., Seitzinger, S., Siewert, J., Signorini, S., Wilkin, J., 2008. Eastern US Continental Shelf Carbon Budget: Integrating Models, Data Assimilation, and Analysis. Oceanography 21, 86–104. https://doi.org/10.5670/oceanog.2008.70

Hunt, C.W., Salisbury, J.E., Vandemark, D., 2011. Contribution of non-carbonate anions to total alkalinity and overestimation of pCO2 in New England and New Brunswick rivers. Biogeosciences 8, 3069–3076. https://doi.org/10.5194/bg-8-3069-2011

(ILO-SLRB) International Lake Ontario-St. Lawrence River Board. 2018. Lake Ontario - St. Lawrence River 2017 High Water - Questions and Answers. International Joint Commission. https://ijc.org/en/loslrb/watershed/faq/2017. Accessed 10/5/2020.

Jiang, Z.-P., Tyrrell, T., Hydes, D.J., Dai, M., Hartman, S.E., 2014. Variability of alkalinity and the alkalinity-salinity relationship in the tropical and subtropical surface ocean. Global Biogeochemical Cycles 28, 729–742. https://doi.org/10.1002/2013GB004678

Joesoef, A., Kirchman, D.L., Sommerfield, C.K., Cai, W.-J., 2017. Seasonal variability of the inorganic carbon system in a large coastal plain estuary. Biogeosciences 14, 4949–4963. https://doi.org/10.5194/bg-14-4949-2017

Jutras, M., C. O. Dufour, A. Mucci, F. Cyr, and D. Gilbert. 2020. Temporal Changes in the Causes of the Observed Oxygen Decline in the St. Lawrence Estuary. Journal of Geophysical Research: Oceans 125: e2020JC016577. doi:https://doi.org/10.1029/2020JC016577

Key, R.M., A. Olsen, S. van Heuven, S. K. Lauvset, A. Velo, X. Lin, C. Schirnick, A. Kozyr, T. Tanhua, M. Hoppema, S. Jutterström, R. Steinfeldt, E. Jeansson, M. Ishi, F. F. Perez, and T. Suzuki. 2015. Global Ocean Data Analysis Project, Version 2 (GLODAPv2), ORNL/CDIAC-162, ND-P093. Carbon Dioxide Information Analysis Center, Oak Ridge National Laboratory, US Department of Energy, Oak Ridge, Tennessee. doi:10.3334/CDIAC/OTG.NDP093_GLODAPv2.

Kuliński, K., Schneider, B., Hammer, K., Machulik, U., Schulz-Bull, D., 2014. The influence of dissolved organic matter on the acid–base system of the Baltic Sea. Journal of Marine Systems 132, 106–115. https://doi.org/10.1016/j.jmarsys.2014.01.011

Land, P.E., Findlay, H.S., Shutler, J.D., Ashton, I.G.C., Holding, T., Grouazel, A., Girard-Ardhuin, F., Reul, N., Piolle, J.-F., Chapron, B., Quilfen, Y., Bellerby, R.G.J., Bhadury, P., Salisbury, J., Vandemark, D., Sabia, R., 2019. Optimum satellite remote sensing of the marine carbonate system using empirical algorithms in the global ocean, the Greater Caribbean, the Amazon Plume and the Bay of Bengal. Remote Sensing of Environment 235, 111469. https://doi.org/10.1016/j.rse.2019.111469

Lee, K., Tong, L.T., Millero, F.J., Sabine, C.L., Dickson, A.G., Goyet, C., Park, G.-H., Wanninkhof, R., Feely, R.A., Key, R.M., 2006. Global relationships of total alkalinity with salinity and temperature in surface waters of the world's oceans. Geophysical Research Letters 33. https://doi.org/10.1029/2006GL027207

Li, Q., Wang, F., Wang, Z.A., Yuan, D., Dai, M., Chen, J., Dai, J., Hoering, K.A., 2013. Automated Spectrophotometric Analyzer for Rapid Single-Point Titration of Seawater Total Alkalinity. Environ. Sci. Technol. 47, 11139–11146. https://doi.org/10.1021/es402421a

Li, X., Bellerby, R.G.J., Wallhead, P., Ge, J., Liu, Jie, Liu, Jing, Yang, A., 2020. A Neural Network-Based Analysis of the Seasonal Variability of Surface Total Alkalinity on the East China Sea Shelf. Front. Mar. Sci. 7. https://doi.org/10.3389/fmars.2020.00219

Loder, J. W. 1998. The coastal ocean off northeastern North America : a large-scale view. The Sea 11: 105–138.

Mathis, J., Cross, J., Evans, W., Doney, S., 2015. Ocean Acidification in the Surface Waters of the Pacific-Arctic Boundary Regions. Oceanography 25, 122–135. https://doi.org/10.5670/oceanog.2015.36

Millero, F.J., Lee, K., Roche, M., 1998. Distribution of alkalinity in the surface waters of the major oceans. Marine Chemistry 60, 111–130. https://doi.org/10.1016/S0304-4203(97)00084-4

Mucci, A., M. Starr, D. Gilbert, and B. Sundby. 2011. Acidification of Lower St. Lawrence Estuary Bottom Waters. Atmosphere-Ocean 49: 206–218. doi:10.1080/07055900.2011.599265

Ohashi, K., and J. Sheng. 2013. Influence of St. Lawrence River discharge on the circulation and hydrography in Canadian Atlantic waters. Continental Shelf Research 58: 32–49. doi:https://doi.org/10.1016/j.csr.2013.03.005.

Olsen, A., Key, R.M., Heuven, S. van, Lauvset, S.K., Velo, A., Lin, X., Schirnick, C., Kozyr, A., Tanhua, T., Hoppema, M., Jutterström, S., Steinfeldt, R., Jeansson, E., Ishii, M., Pérez, F.F., Suzuki, T., 2016. The Global Ocean Data Analysis Project version 2 (GLODAPv2) – an internally consistent data product for the world ocean. Earth System Science Data 8, 297–323. https://doi.org/10.5194/essd-8-297-2016

Pershing, A. J., M. A. Alexander, C. M. Hernandez, and others. 2015. Slow adaptation in the face of rapid warming leads to collapse of the Gulf of Maine cod fishery. Science 350: 809–812. doi:10.1126/science.aac9819.

Pershing, A., A. Dayton, B. Franklin, and B. Kennedy. 2018. Evidence for Adaptation from the 2016 Marine Heatwave in the Northwest Atlantic Ocean. Oceanog 31. doi:10.5670/oceanog.2018.213.

Pierrot, D., Neill, C., Sullivan, K., Castle, R., Wanninkhof, R., Lüger, H., Johannessen, T., Olsen, A., Feely, R.A., Cosca, C.E., 2009. Recommendations for autonomous underway pCO2 measuring systems and data-reduction routines. Deep Sea Research Part II: Topical Studies in Oceanography, Surface Ocean CO2 Variability and Vulnerabilities 56, 512–522. https://doi.org/10.1016/j.dsr2.2008.12.005

Rasmussen, L.L., Gawarkiewicz, G., Owens, W.B., Lozier, M.S., 2005. Slope water, Gulf Stream, and seasonal influences on southern Mid-Atlantic Bight circulation during the fall-winter transition. Journal of Geophysical Research: Oceans 110. https://doi.org/10.1029/2004JC002311

Reul, N., Grodsky, S.A., Arias, M., Boutin, J., Catany, R., Chapron, B., D'Amico, F., Dinnat, E., Donlon, C., Fore, A., Fournier, S., Guimbard, S., Hasson, A., Kolodziejczyk, N., Lagerloef, G., Lee, T., Le Vine, D.M., Lindstrom, E., Maes, C., Mecklenburg, S., Meissner, T., Olmedo, E., Sabia, R., Tenerelli, J., Thouvenin-Masson, C., Turiel, A., Vergely, J.L., Vinogradova, N., Wentz, F., Yueh, S., 2020. Sea surface salinity estimates from spaceborne L-band radiometers: An overview of the first decade of observation (2010–2019). Remote Sensing of Environment 242, 111769. https://doi.org/10.1016/j.rse.2020.111769

Salisbury, J., Green, M., Hunt, C., Campbell, J., 2008. Coastal Acidification by Rivers:A Threat to Shellfish? Eos Trans. AGU 89, 513–513. https://doi.org/10.1029/2008EO500001

Salisbury, J., Vandemark, D., Jönsson, B., Balch, W., Chakraborty, S., Lohrenz, S., Chapron, B., Hales, B., Mannino, A., Mathis, J., Reul, N., Signorini, S., Wanninkhof, R., Yates, K., 2015. How Can Present and Future Satellite Missions Support Scientific Studies that Address Ocean Acidification? Oceanography 25, 108–121. https://doi.org/10.5670/oceanog.2015.35

Salisbury, J.E., Jönsson, B.F., 2018. Rapid warming and salinity changes in the Gulf of Maine alter surface ocean carbonate parameters and hide ocean acidification. Biogeochemistry 141, 401–418. https://doi.org/10.1007/s10533-018-0505-3

Seelmann, K., Aßmann, S., Körtzinger, A., 2019. Characterization of a novel autonomous analyzer for seawater total alkalinity: Results from laboratory and field tests. Limnology and Oceanography: Methods 17, 515–532. https://doi.org/10.1002/lom3.10329

Sharp, J. D., and R. H. Byrne. 2020. Interpreting measurements of total alkalinity in marine and estuarine waters in the presence of proton-binding organic matter. Deep Sea Research Part I: Oceanographic Research Papers 165: 103338. doi:10.1016/j.dsr.2020.103338

Sherwood, O. A., M. F. Lehmann, C. J. Schubert, D. B. Scott, and M. D. McCarthy. 2011. Nutrient regime shift in the western North Atlantic indicated by compound-specific δ15N of deep-sea gorgonian corals. PNAS 108: 1011–1015. doi:10.1073/pnas.1004904108

Signorini, S.R., Mannino, A., Najjar, R.G., Friedrichs, M.A.M., Cai, W.-J., Salisbury, J., Wang, Z.A., Thomas, H., Shadwick, E., 2013. Surface ocean pCO2 seasonality and sea-air CO2 flux estimates for the North American east coast. J. Geophys. Res. Oceans 118, 5439–5460. https://doi.org/10.1002/jgrc.20369

Takahashi, T., Sutherland, S.C., Chipman, D.W., Goddard, J.G., Ho, C., Newberger, T., Sweeney, C., Munro, D.R., 2014. Climatological distributions of pH, pCO2, total CO2, alkalinity, and CaCO3 saturation in the global surface ocean, and temporal changes at selected locations. Marine Chemistry 164, 95–125. https://doi.org/10.1016/j.marchem.2014.06.004

Thomas, H., Schiettecatte, L.-S., Suykens, K., Koné, Y.J.M., Shadwick, E.H., Prowe, A.E.F., Bozec, Y., de Baar, H.J.W., Borges, A.V., 2009. Enhanced ocean carbon storage from anaerobic alkalinity generation in coastal sediments. Biogeosciences 6, 267–274. https://doi.org/10.5194/bg-6-267-2009

Townsend, D.W., Thomas, A.C., Mayer, L.M., Thomas, M., Quinlan, J., 2006. Oceanography of the Northwest Atlantic Continental Shelf, in: The Sea. Harvard University Press, pp. 119–168.

Townsend, D. W., N. R. Pettigrew, M. A. Thomas, M. G. Neary, D. J. McGillicuddy, and J. O'Donnell. 2015. Water Masses and Nutrient Sources to the Gulf of Maine. Journal of marine research 73: 93–122. doi:10.1357/002224015815848811.

Wallace, R.B., Baumann, H., Grear, J.S., Aller, R.C., Gobler, C.J., 2014. Coastal ocean acidification: The other eutrophication problem. Estuarine, Coastal and Shelf Science 148, 1–13. https://doi.org/10.1016/j.ecss.2014.05.027

Wang, Z.A., Wanninkhof, R., Cai, W.-J., Byrne, R.H., Hu, X., Peng, T.-H., Huang, W.-J., 2013. The marine inorganic carbon system along the Gulf of Mexico and Atlantic coasts of the United States: Insights from a transregional coastal carbon study. Limnol. Oceanogr. 58, 325–342. https://doi.org/10.4319/lo.2013.58.1.0325

Wang, Z.A., Kroeger, K.D., Ganju, N.K., Gonneea, M.E., Chu, S.N., 2016. Intertidal salt marshes as an important source of inorganic carbon to the coastal ocean. Limnol. Oceanogr. 61, 1916–1931. https://doi.org/10.1002/lno.10347

Wanninkhof, R., Barbero, L., Byrne, R., Cai, W.-J., Huang, W.-J., Zhang, J.-Z., Baringer, M., Langdon, C., 2015. Ocean acidification along the Gulf Coast and East Coast of the USA. Continental Shelf Research 98, 54–71. https://doi.org/10.1016/j.csr.2015.02.008

Xu, Y.-Y., W.-J. Cai, Y. Gao, and others. 2017. Short-term variability of aragonite saturation state in the central Mid-Atlantic Bight. Journal of Geophysical Research: Oceans 122: 4274–4290. doi:10.1002/2017JC012901

Yang, B., Byrne, R.H., Lindemuth, M., 2015. Contributions of organic alkalinity to total alkalinity in coastal waters: A spectrophotometric approach. Marine Chemistry 176, 199–207. https://doi.org/10.1016/j.marchem.2015.09.008

Yao, W., Byrne, R.H., 1998. Simplified seawater alkalinity analysis. Deep Sea Research Part I: Oceanographic Research Papers 45, 1383–1392. https://doi.org/10.1016/S0967-0637(98)00018-1

Zeebe, R.E., 2012. History of Seawater Carbonate Chemistry, Atmospheric CO2, and Ocean Acidification. Annual Review of Earth and Planetary Sciences 40, 141–165. https://doi.org/10.1146/annurev-earth-042711-105521

Zweng, M.M, Reagan, J.R., Seidov, D., Boyer, T.P. , Locarnini, R.A., Garcia, H.E., Mishonov, A.V., Baranova, O.K., Weathers, K.W., Paver, C.R., Smolyar, I.V., 2019. World Ocean Atlas 2018, Volume 2: Salinity. A. Mishonov, Technical Editor, NOAA Atlas NESDIS 82, 50pp.

Figures:

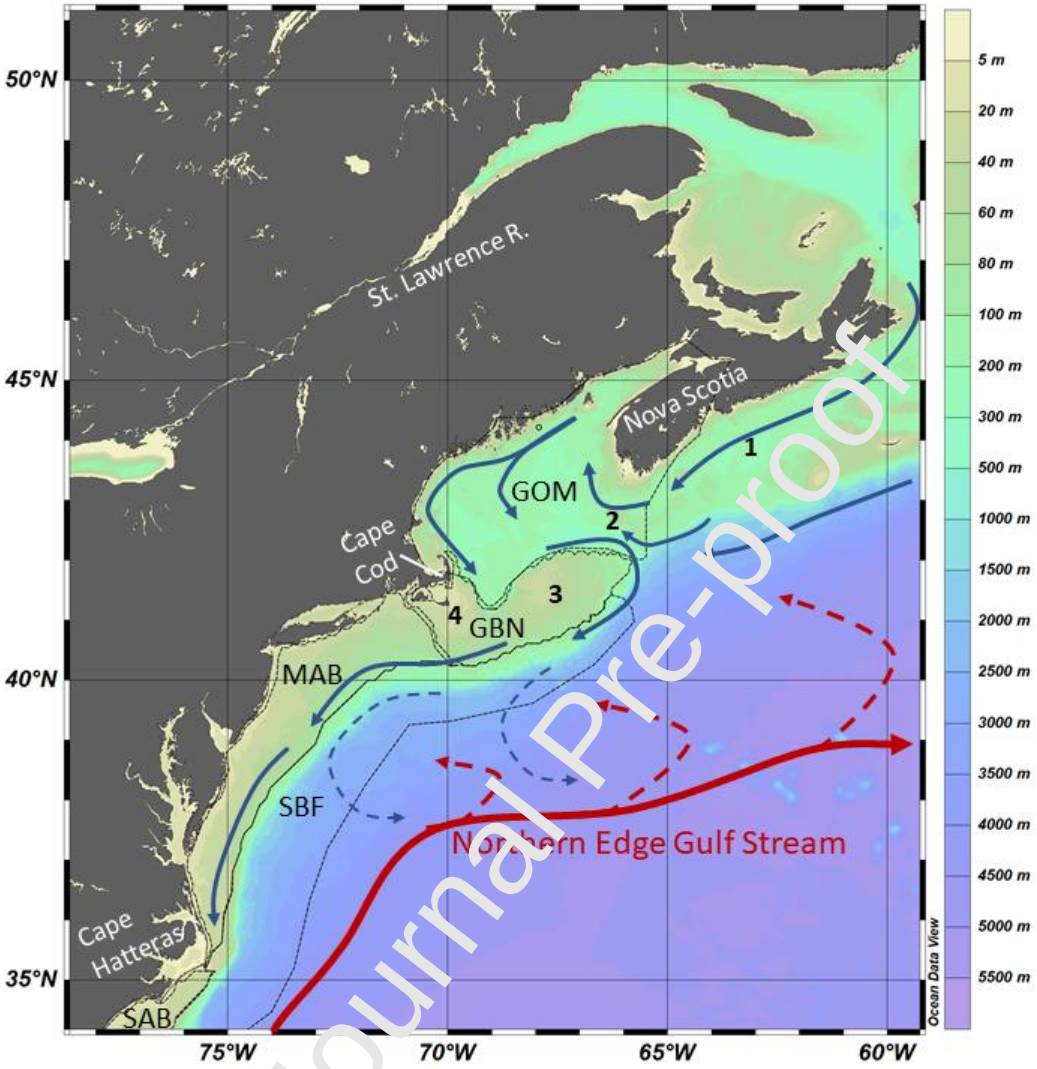

Figure 1. Study area map with bathymetry, adapted from Townsend et al. (2006), with study subregions outlined. The study subregions are the Gulf of Maine (GOM), George's Bank/Nantucket Shoals (GBN), Middle Atlantic Bight (MAB), and Shelf-Break Front (SBF). The South Atlantic Bight (SAB) region is also shown south of Cape Hatteras. Numbers indicate specific locations found in the text: 1: Scotian Shelf; 2: Northeast Channel; 3: George's Bank; 4: Great South Channel. General positions of major currents are shown as red and blue arrows. The position of the Gulf Stream's northern edge is approximate, dashed red and blue arrows show the presence of cross-shelf mixing and not locations of actual currents.

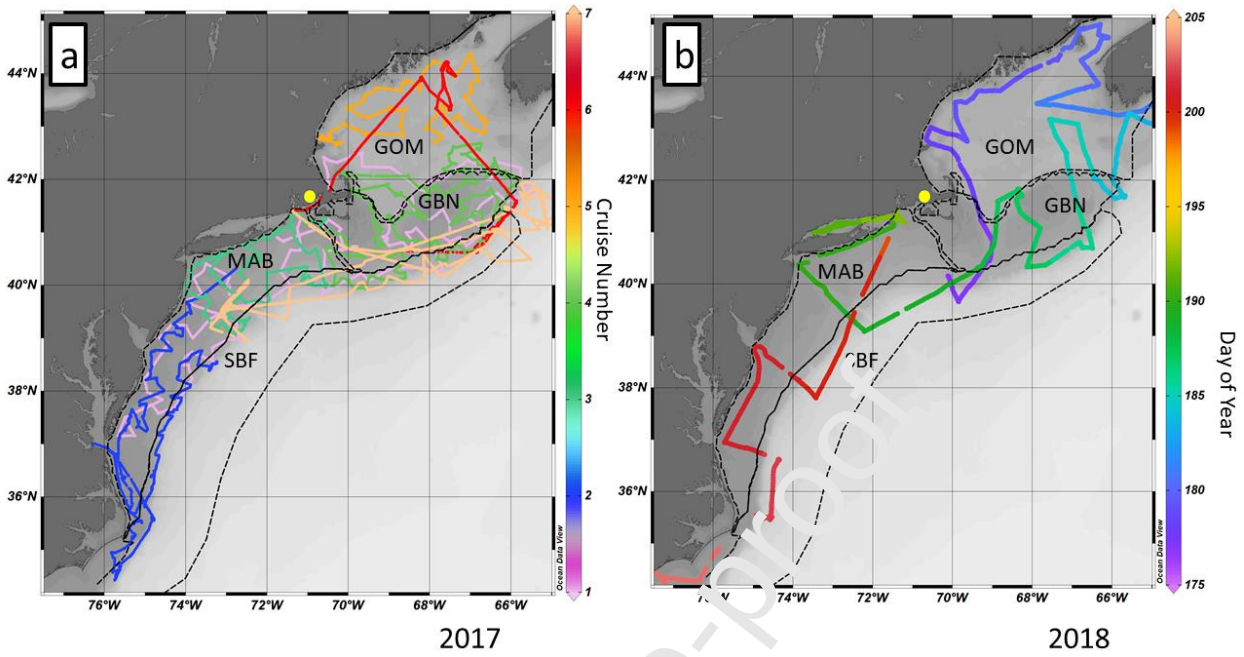

Figure 2. Map of 2017 (panel a) and 2018 (panel b) cruise tracks presented in this work with East Coast regions outlined. Note that colors in panel a identify the cruise number (see Table 1), while colors in panel b indicate day-of-year. The NOAA Ship *Henry B. Bigelow*'s home port of Newport Rhode Island USA is shown as a yellow circle. A summary of these cruises is provided in Table 1.

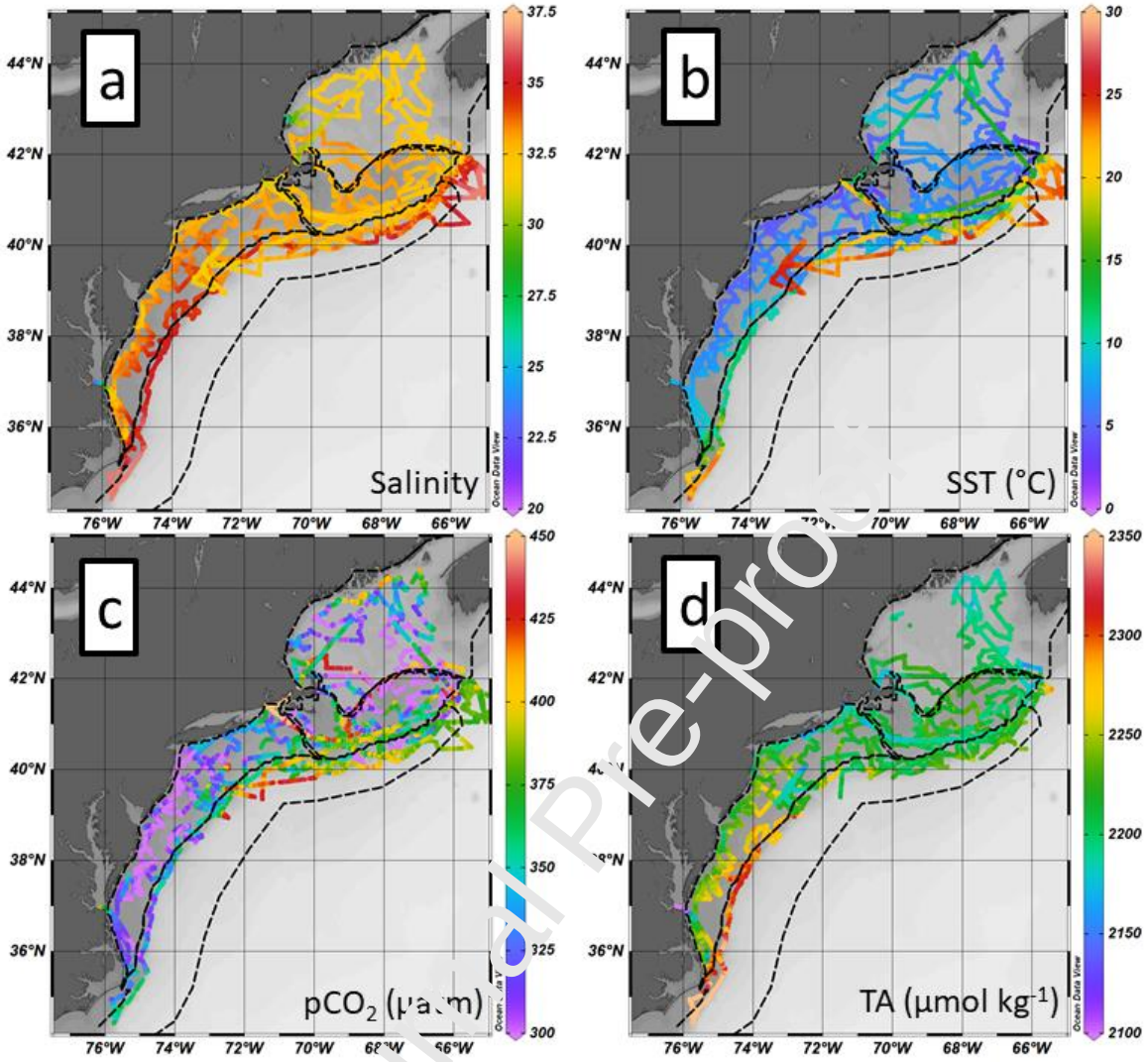

Figure 3. Maps of all surface data collected underway in 2017. Parameters shown are sea surface salinity (panel a), temperature (panel b, degrees Celsius), pCO_2 (panel c, µatm), and HydroFIA TA (panel d, µmol kg^{-1}). Black lines represent regional boundaries, see text and Figure 1. Color bars correspond to the data point colors in each panel and are scaled identically to those in Figure 4.

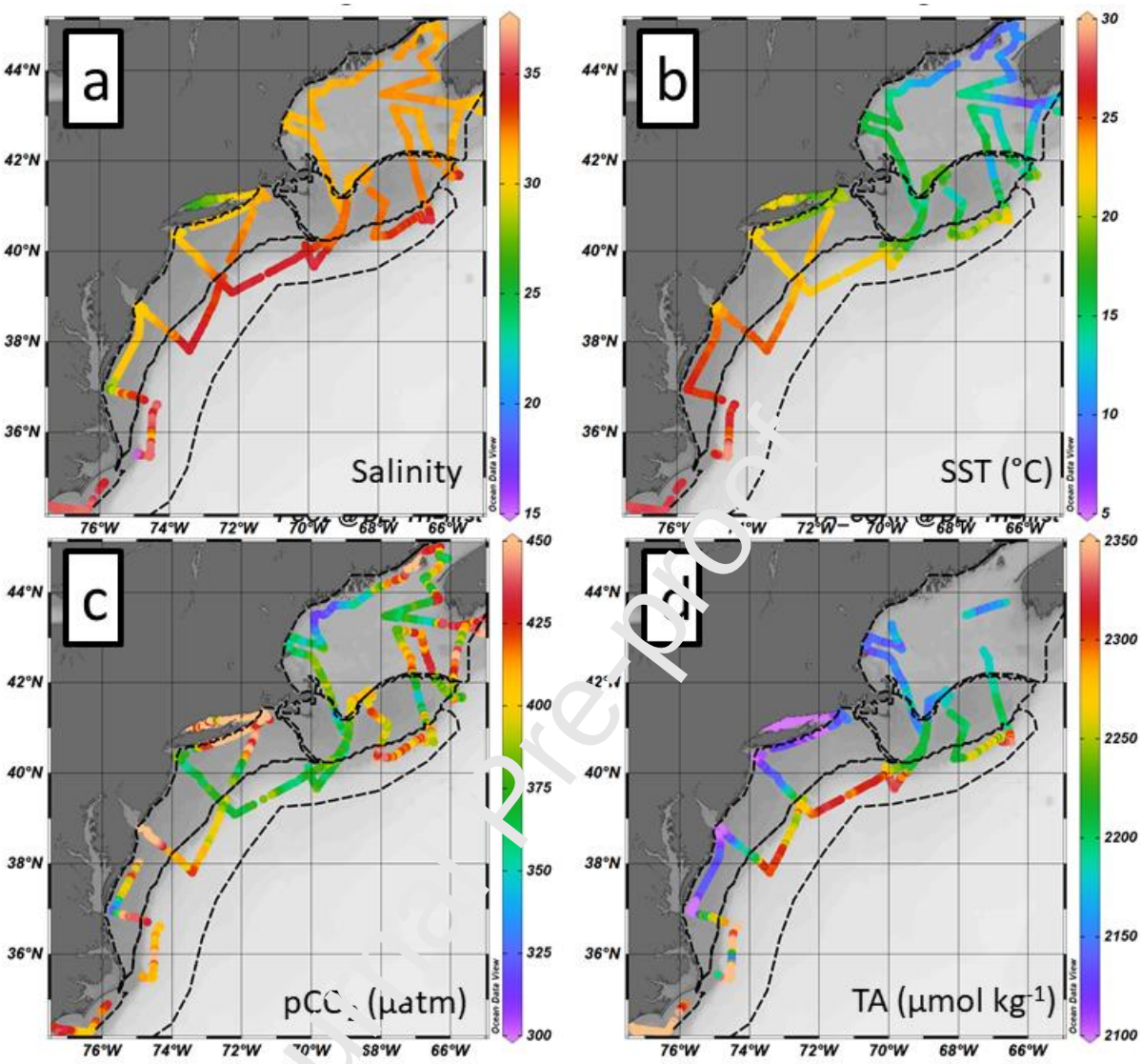

Figure 4. Maps of ECOA 2018 sea surface salinity (panel a), temperature (panel b, degrees Celsius), pCO_2 (panel c, µatm), and HydroFIA TA (panel d, µmol kg^{-1}). Black lines represent regional boundaries, see text and Figure 1. Color bars correspond to the data point colors in each panel and are scaled identically to those in Figure 3. The low-salinity, low-alkalinity data shown in Long Island Sound do not fall within the bounds of the regions discussed in this study, and thus do not influence the discussion of regional findings.

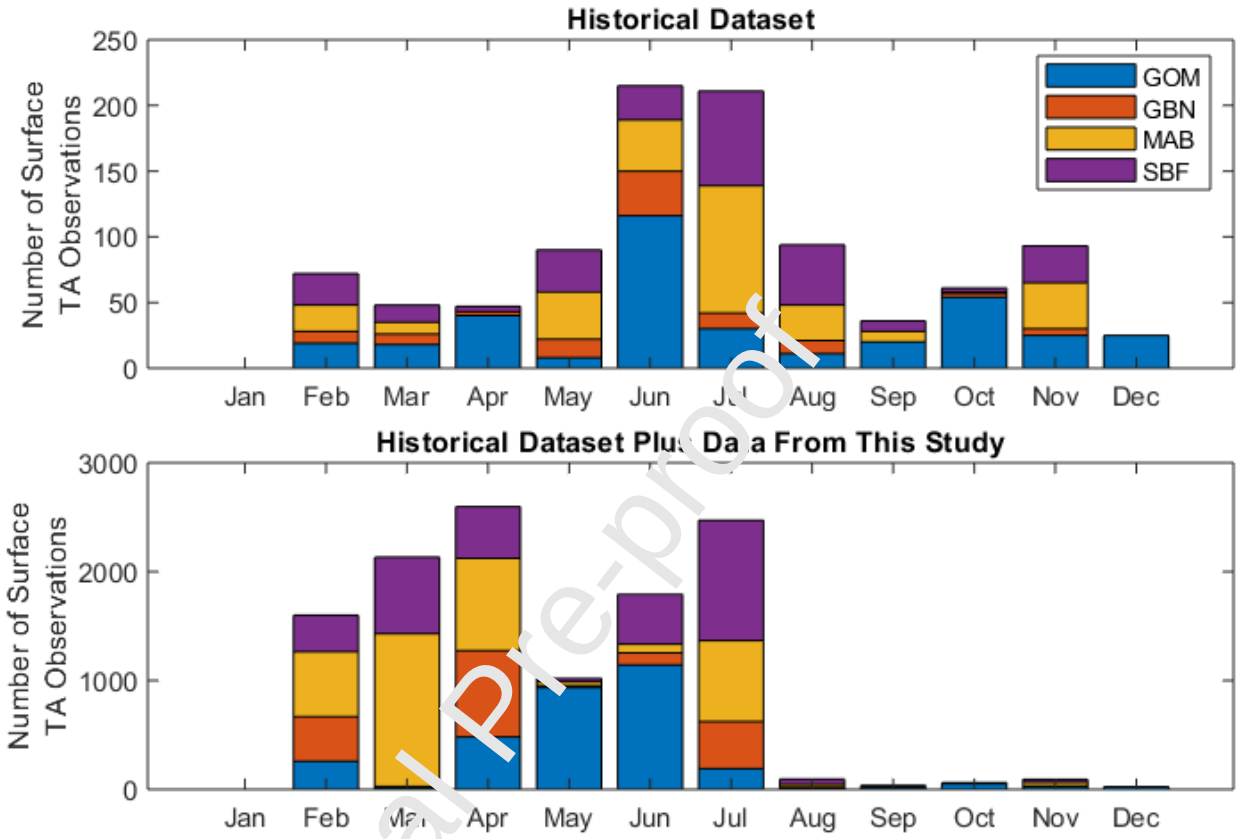

Figure 5. Monthly counts of regional surface TA measurements. The top panel shows the counts for each region from the historical dataset described in Section 2.4. The bottom panel shows counts for each region once the HydroFIA TA system measurements from 2017 and 2018 described in this study are included. Note the roughly one order of magnitude difference in y-axis scales between top and bottom panels.

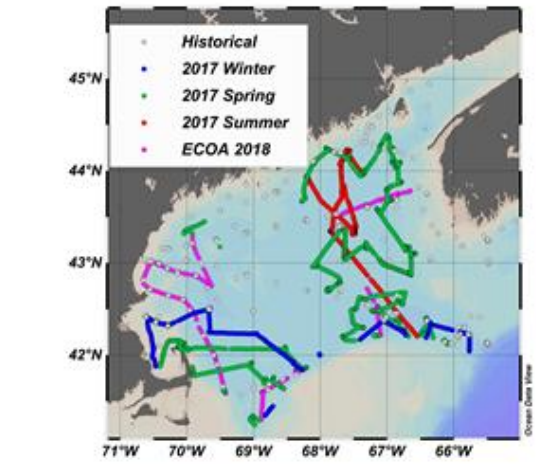

	Slope	T-Alk⁰	R²	RMSE	n
Winter2017	41.3 (±0.4)	852 (±13)	0.98	3	224
Spring2017	24.3 (±0.4)	1415 (±14)	0.77	5	969
Summer2017	26.2 (±0.6)	1357 (±18)	0.87	4	347
ECOA2018	62.6 (±0.9)	178 (±28)	0.97	4	185
Historical	47.6 (±0.7)	643 (±22)	0.93	12	378

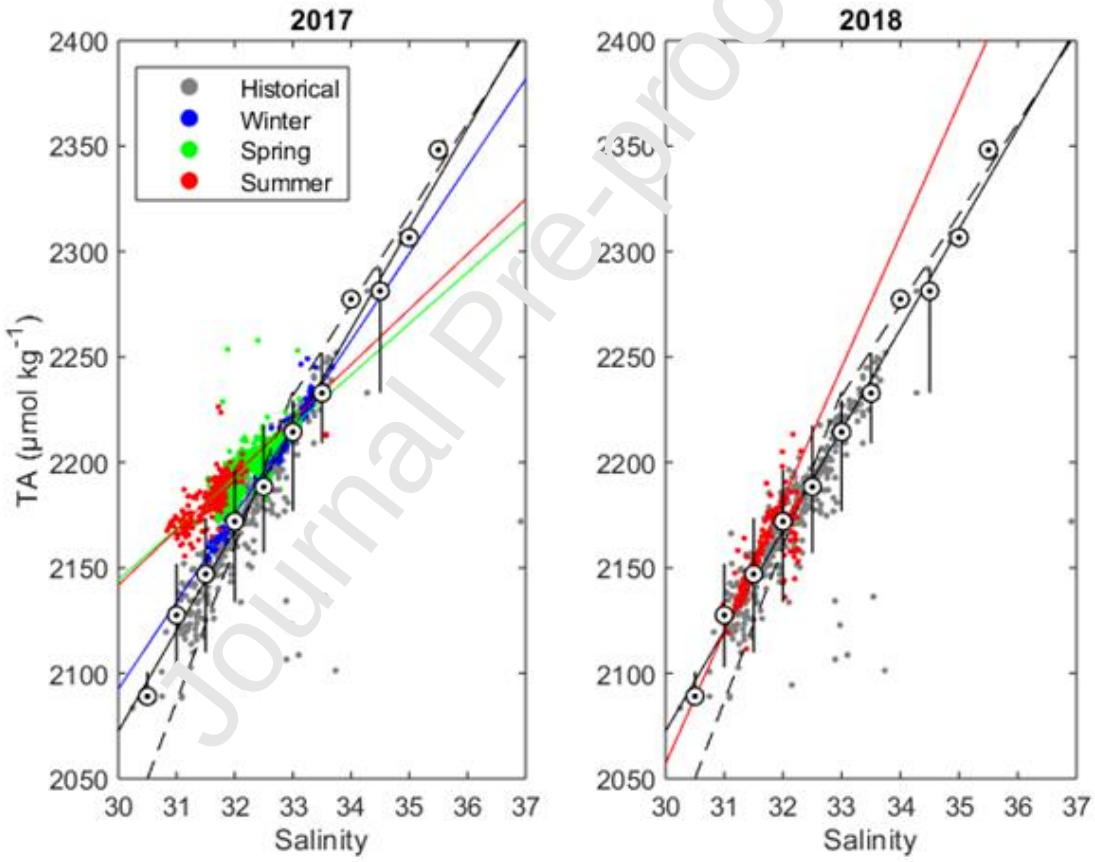

Figure 6. Gulf of Maine seasonal and historic TA and salinity data. Upper-left panel shows the locations of surface data collections. Lower-left and lower-right panels show scatterplots of seasonal salinity and TA from 2017 and the 2018 ECOA-2 cruise, respectively. Note that the historical data are inclusive of all seasons. For reference, the solid line indicates the robust linear regression of historical data; the dashed lines indicate the mixing lines described by Cai et al.

(2010). The slope and TA^0 from Cai et al. (2010) are 65.8 and 75.1±291.2 µmol kg^{-1}, respectively, for sample salinities less than 31.75. The slope and TA^0 from Cai et al. (2010) are 39.1 and 932.7±16.5 µmol kg^{-1}, respectively, for sample salinities greater than 31.75. Whisker plots show the median TA (white circles) at 0.5-salinity intervals of historical data; whiskers indicate the range of TA over each 0.5-salinity interval. Colored lines show the linear regression of measurements for each season. The table in the upper-right lists the linear regression slope and intercept coefficients (with standard errors in parentheses), as well as the r^2, RMSE and *n* statistics. The p-values for all regressions were much less than 0.01.

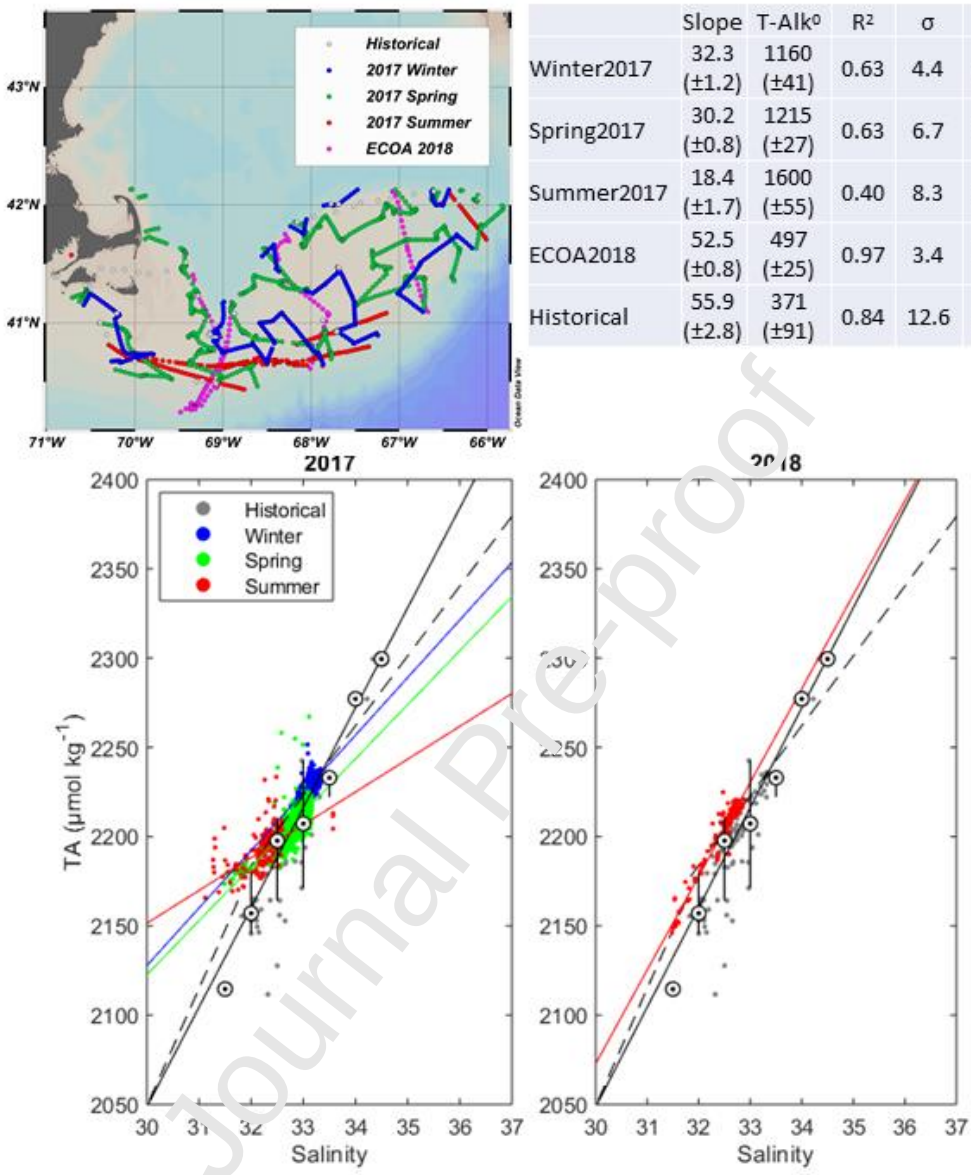

	Slope	T-Alk⁰	R²	σ	n
Winter2017	32.3 (±1.2)	1160 (±41)	0.63	4.4	391
Spring2017	30.2 (±0.8)	1215 (±27)	0.63	6.7	780
Summer2017	18.4 (±1.7)	1600 (±55)	0.40	8.3	181
ECOA2018	52.5 (±0.8)	497 (±25)	0.97	3.4	196
Historical	55.9 (±2.8)	371 (±91)	0.84	12.6	98

Figure 7. George's Bank-Nantucket Shoals (GBN) seasonal and historic TA and salinity data. See the caption of Figure 8 for detailed figure explanations. For reference, the solid line indicates the robust linear regression of historical data; the dashed lines indicate the "Woods Hole Transect" mixing lines described by Cai et al. (2010). The slope and TA^0 from Cai et al. (2010) are 73.4 and (-188.7±92.3) µmol kg^{-1}, respectively, for sample salinities less than 33. The slope and TA^0 from

Cai et al. (2010) are 43.1 and 809.2±60.9 μmol kg^{-1}, respectively, for sample salinities greater than 33. The p-values for all regressions presented in the table were much less than 0.01.

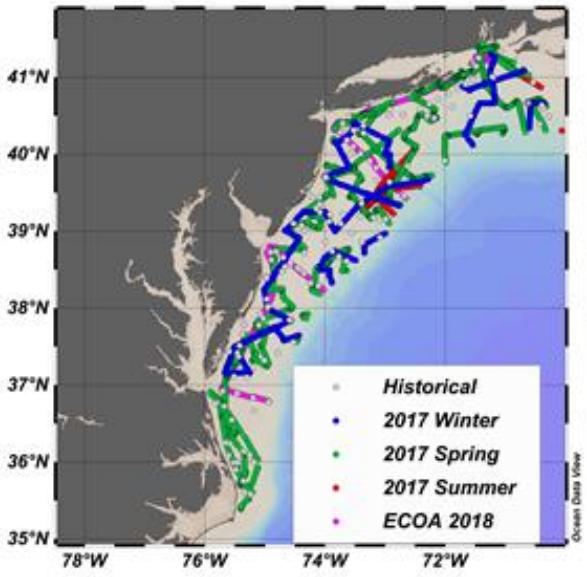

	Slope	T-Alk⁰	R²	σ	n
Winter	40.8 (±0.7)	880 (±25)	0.84	9.2	557
Spring	44.1 (±0.4)	763 (±14)	0.83	11.7	2210
Summer	14.5 (±0.3)	1726 (±8.1)	0.93	1.9	242
ECOA2018	38.5 (±1.2)	935 (±39)	0.83	18.2	193
Historical	43.7 (±1.0)	765 (±3.)	0.87	18.1	272

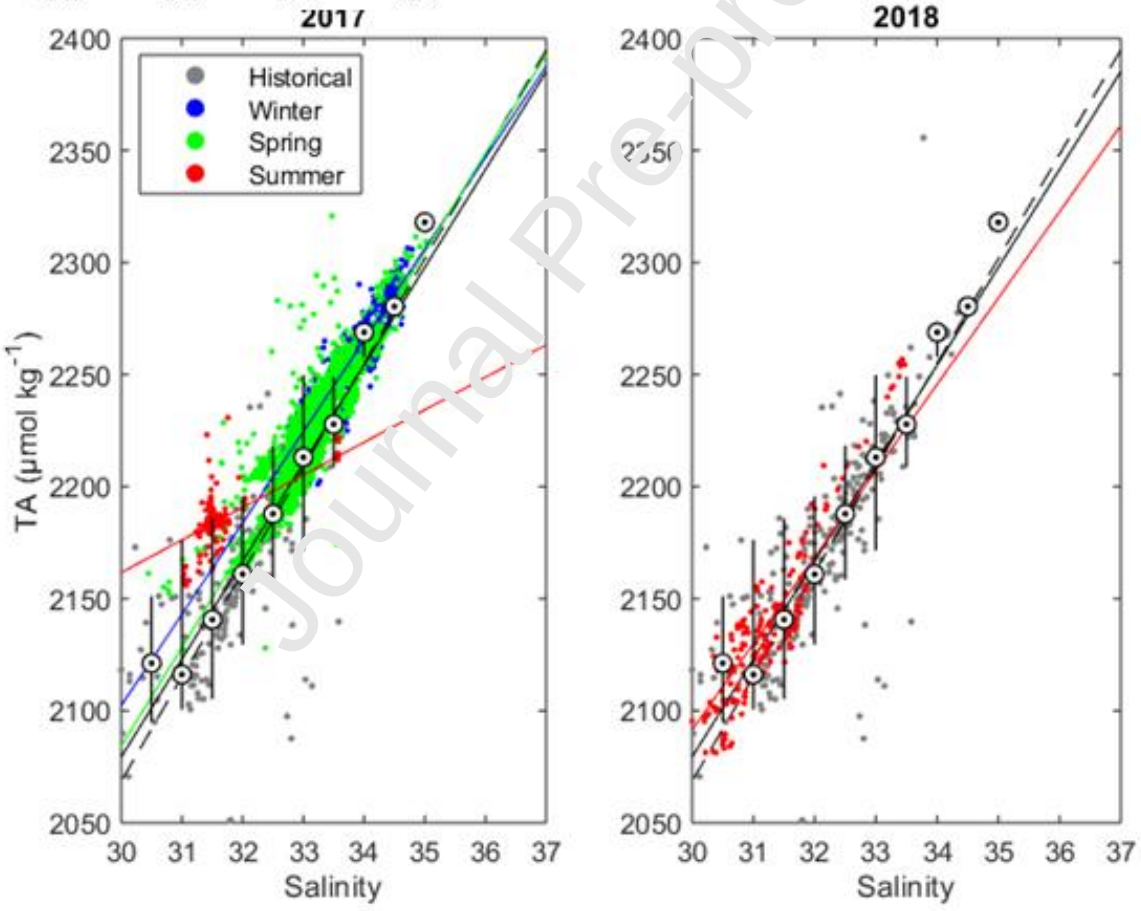

Figure 8. Middle Atlantic Bight (MAB) seasonal and historic TA and salinity data. See the caption of Figure 8 for detailed figure explanations. For reference, the solid line indicates the robust

linear regression of historical data; the dashed line indicates the mixing line described by Cai et al. (2010). The slope and TA^0 from Cai et al. (2010) are 46.6 and 670.6±12.3 µmol kg^{-1}, respectively. The p-values for all regressions presented in the table were much less than 0.01.

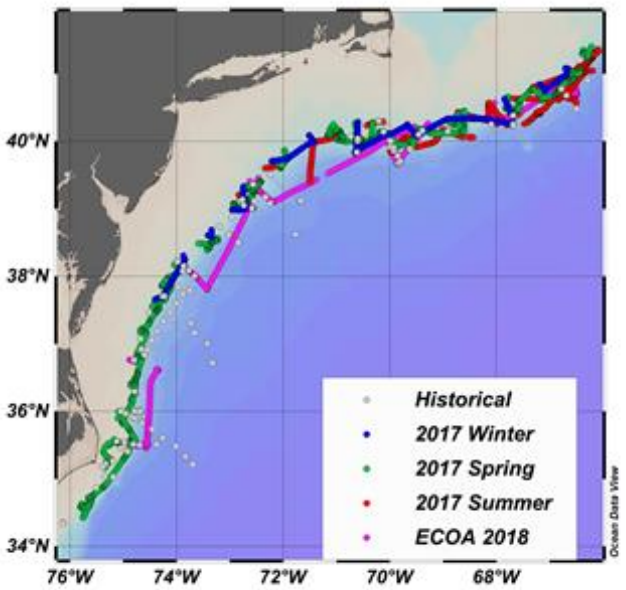

	Slope	T-Alk⁰	R²	σ	n
Winter	44.2 (±0.3)	761 (±11)	0.98	4.9	303
Spring	42.2 (±0.2)	821 (±8)	0.97	9.7	1139
Summer	21.7 (±0.4)	1497 (±13)	0.82	6.4	704
ECOA2018	46.9 (±0.2)	687 (±8)	0.99	4.8	353
Historical	47.9 (±0.5)	638 (±18)	0.97	10.8	256

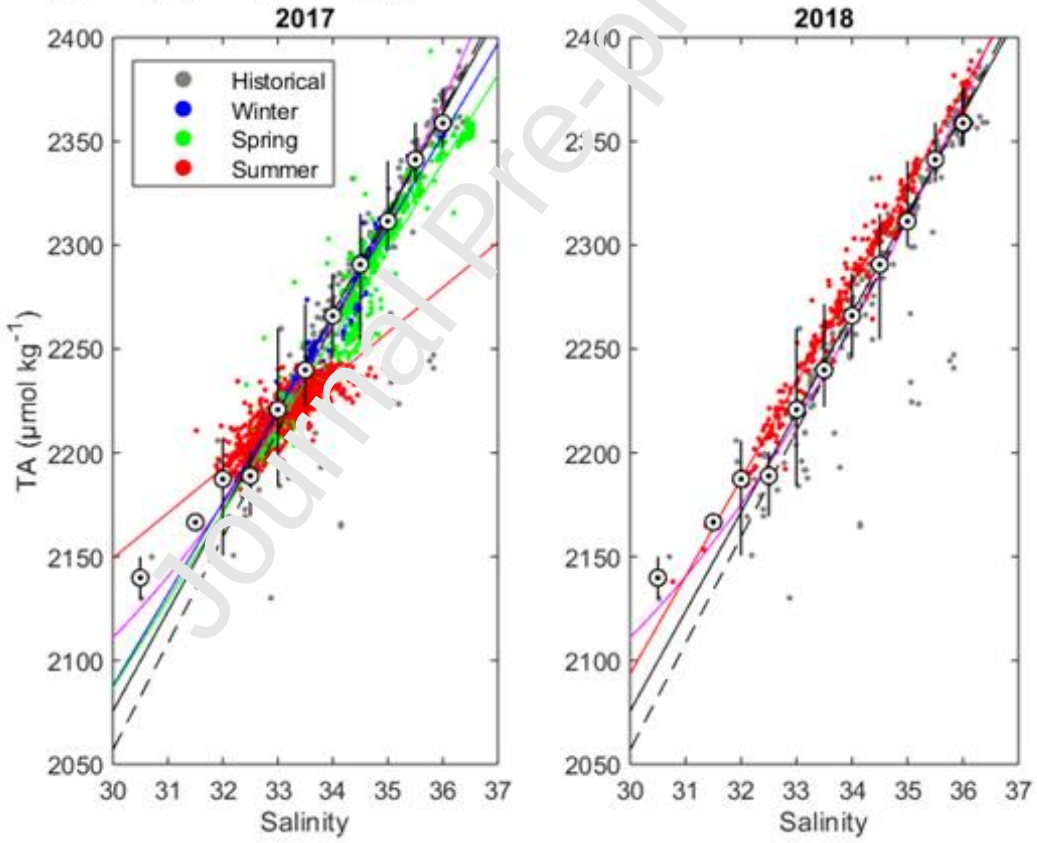

Figure 9. Shelf Break Front (SBF) seasonal and historic TA and salinity data. See the caption of Figure 8 for detailed figure explanations. For reference, the solid line in the lower two panels

indicates the robust linear regression of historical data; the magenta line indicates the mixing line described by Lee et al. (2006, $TA = 2305 + 53.97*(S - 35) + 2.74* (S - 35)^2 - 1.16 (SST - 20) - 0.040 (SST - 20)^2$, where S is salinity and SST is surface temperature) and the dashed black line indicates the mixing line described by Millero et al. (1998, $TA=S*51.24 + 520.1$, where S is salinity). The p-values for all regressions presented in the table were much less than 0.01.

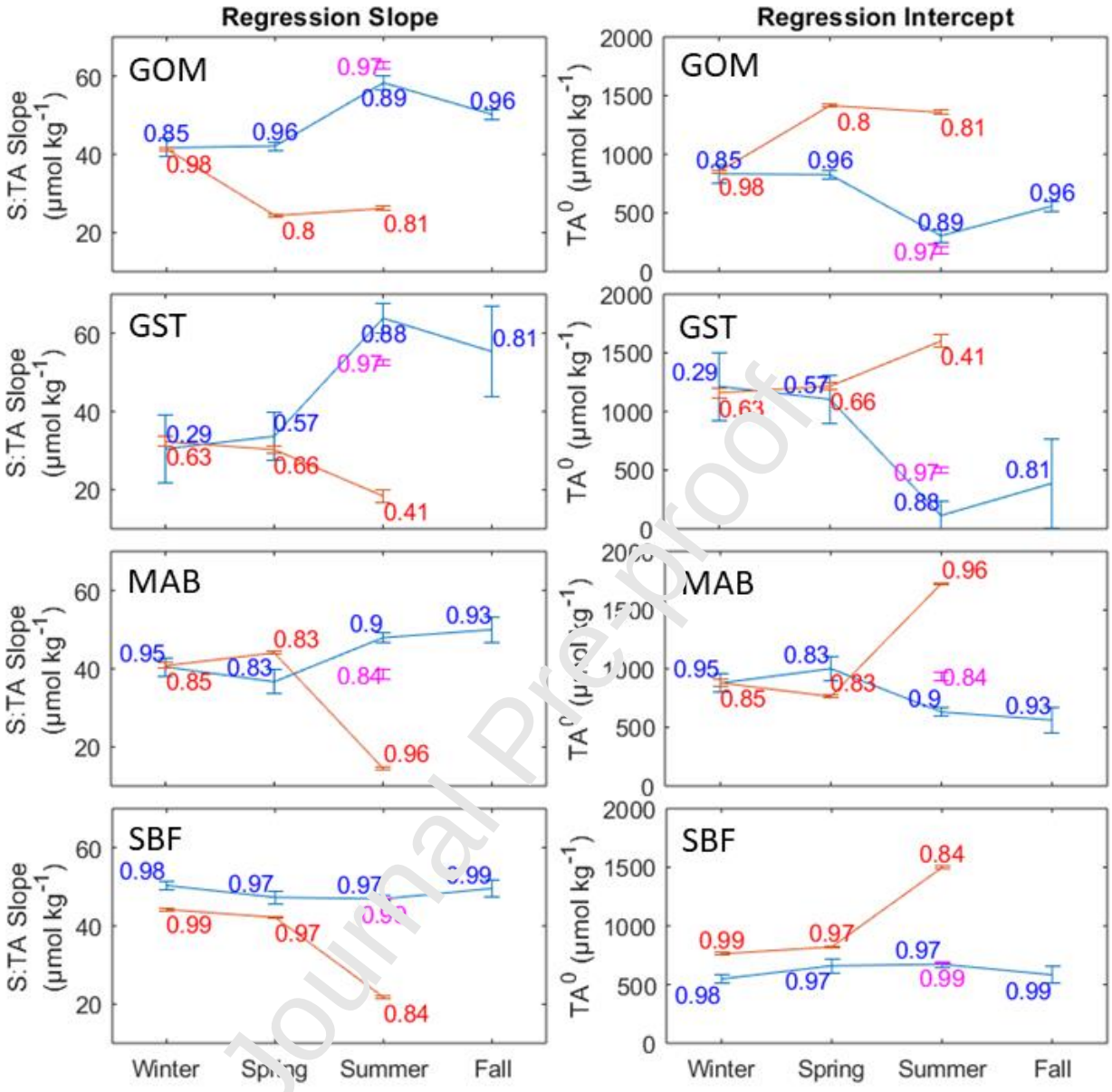

Figure 10. Seasonal, regional slope and y-intercept (TA^0) statistics produced from a robust linear regression method (see Section 2.3). Error bars show the standard error around each value, and numbers beside each point correspond to the r^2 statistic. Blue lines and r^2 values were calculated from the historical dataset (see Section 2.4), red lines and r^2 values were calculated from the 2017 HydroFIA TA data, and magenta lines and r^2 were calculated from the 2018 ECOA HydroFIA TA data.

Table 1. Cruise summaries for the 2017 and ECOA-2 efforts, all aboard the NOAA Ship *Henry B. Bigelow*.

	Dates	Cruise Duration (days)	Latitude Range (°N)	Longitude Range (°W)	n TA observations	TA Range (µmol kg-1)	Salinity Range	T Range (degrees C)
Cruise 1	Feb 11 - Feb 22, 2017	12	37.15 - 42.51	-75.67 - -65.42	1585	2136 - 2356	31.46 - 36.08	2.495 - 14.969
Cruise 2	Mar 7 - Mar 22, 2017	16	34.43 - 40.32	-76.29 - -72.76	1575	1888 - 2400	22.97 - 36.55	4.765 - 24.003
Cruise 3	Mar 28 - Apr 6, 2017	10	39.04 - 41.48	-74.01 - -70.51	154	2068 - 2332	30.11 - 34.88	3.728 - 11.209
Cruise 4	Apr 12 - Apr 26, 2017	15	39.93 - 42.68	-71.38 - -65.76	16[illegible]9	2171 - 2294	31.49 - 34.83	2.1483 - 11.211
Cruise 5	May 5 - May 11, 2017	7	42.64 - 44.39	-70.74 - -66.57	5[illegible]6	2169 - 2217	31.2 - 32.52	4.504 - 8.167
Cruise 6	Jun 10 - Jun 22, 2017	13	40.62 - 44.23	-70.72 - -65.8[illegible]	897	2156 - 2262	30.84 - 35.28	9.010 - 15.044
Cruise 7	Jul 6 - Jul 19, 2017	14	39.20 - 41.76	-73.38 - -65.2[illegible]	1134	2156 - 2274	31.02 - 36.58	11.317 - 25.457
ECOA-2	Jun 26 - Jul 29, 2018	34	26.81 - 45.01	-[illegible]0.9[illegible] -61.4	1656	2001 - 2403	26.61 - 36.42	6.38 - 31.77

Table 2. Analytical uncertainties of paired discrete bottle sample and HydroFIA TA analyses. Paired sampling was conducted during Cruise 1 (Feb 11-22, 2017) and the 2018 ECOA-2 cruise. Discrete TA analyses were performed by two laboratories: the NOAA Atlantic Oceanographic and Meteorological Laboratory ("AOML") and the laboratory of Dr. Wei-Jun Cai at the University of Delaware ("U.Del."). AOML analyses used CRM Batches 129 and 144; U.Del. used Batch 173. The HydroFIA CRM was Batch 159 in 2017 and 173 during ECOA-2. AOML samples were preserved and analyzed three weeks after Cruise 1, U.Del. samples were not preserved and analyzed on board within 24 hours of collection.

	2017 Cruise 1	ECOA-2
Analyzing laboratory	AOML	U.Del.
σ (CRM)	±2.0	±1.2
RMSE (CRM)	±1.8	±1.2
u(CRM)	±0.52	±0.64
$u(bias)_{CRM}$	±1.9	±1.4
u_c	±2.8	±1.8
RMSE (rep)	±5.6	±1.5
u(rep)	±5.2	±0.9
n_{CRM}, n_{rep}	10,9	81, 27
σ (HydroFIA CRM)	±2.0	±1.4
RMSE (HydroFIA CRM)	±1.3	±3.8
u (HydroFIA CRM)	±0.59	±0.64
u(bias) HydroFIA	±1.4	±3.9
$u_{c\ (HydroFIA)}$	±2.4	±4.1
n	9	25
RMSE, paired samples	±7.0	±10.3
u(other), paired samples	±2.9	±9.2

Table 3. Regional summary statistics for 2017 and ECOA-2 data. In order, the data presented for each parameter (e.g. salinity, temperature) are: the regional range of each observation type (minimum and maximum), the statistical mean, one standard deviation around the mean, and total number of measurements in each region. The mean, standard deviation, and measurement number are grouped in parentheses. Results from the 2018 ECOA-2 cruise are in shaded rows. Bold values indicate the highest and lowest values observed for each parameter in 2017 and 2018.

	Dates	Salinity	Temperature (degrees C)	pCO2 (µatm)	TA (µmol kg^{-1})
GOM	Feb 19 - Jun 21, 2017	**24.13** - 33.68 (31.95±0.85 n=2244)	2.87 - 14.54 (3.60±3.26 n=2271)	229 - 448 (335±43 n=1546)	2154 - 2258 (2196±15 n=1857)
GOM	Jun 27 - Jul 7, 2018	30.94 - 32.34 (31.72±0.31 n=497)	**6.37** - 18.91 (13.17±2.96 n=497)	310 - 457 (390±33 n=484)	2112 - 2213 (2158±18 n=185)
GBN	Feb 16 - Jul 19, 2017	31.12 - 33.77 (32.75±0.42 n=1451)	**2.15** - 20.94 (7.96±3.87 n=1460)	202 - 564 (346±54 n=1353)	2166 - 2267 (2211±16 n=1196)
GBN	Jun 26 - Jul 8, 2018	31.48 - 32.80 (32.46±0.33 n=212)	10.14 - 18.71 (15.74±1.87 n=212)	333 - 441 (378±16 n=201)	2146 - 2225 (2204±17 n=196)
MAB	Feb 11 - Jul 19, 2017	28.99 - 35.04 (32.98±0.85 n=3285)	3.73 - **25.45** (9.18±6.16 n=3288)	255 - **599** (331±36 n=3009)	**2087** - **2400** (2225±31 n=2699)
MAB	Jul 8 - Jul 20, 2018	**26.61** - 33.47 (31.19±1.07 n=219)	17.85 - 26.28 (22.23±2.38 n=219)	**307** - **534** (421±52 n=189)	**2001** - 2257 (2132±43 n=193)
SBF	Feb 12 - Jul 18, 2017	31.26 - **36.55** (33.76±1.12 n=2564)	4.85 - 25.19 (13.57±6.1 n=2570)	**196** - 437 (352±42 n=2353)	2183 - 2397 (2247±44 n=2116)
SBF	Jun 26 - Jul 21, 2018	30.77 - **36.20** (34.08±1.06 n=353)	14.37 - **29.14** (22.49±3.1 n=353)	352 - 480 (398±27 n=325)	2138 - **2389** (2285±50 n=325)

Table 4. Deviations between 2017 TA observations and TA estimates from regional models. The models used are those of Cai et al. (2010) and Lee et al. (2006). All differences are calculated as model-derived TA subtracted from the observed TA, thus positive values indicate model underestimate relative to the observed TA. Negative values are shown in parentheses. The third column ("Difference σ") lists one standard deviation of the calculated differences for each region, and the fourth column lists the number of observations. All values are μmol kg^{-1}.

	Difference from Cai et al. (2010)			
Region	Mean Difference	Range of Difference	Difference σ	n
GOM	8	(-33) - 74	14	1545
GBN	-5	(-52) - 90	16	1353
MAB	12	(-60) - 97	16	3009
SBF	-	-	-	

	Difference from Lee et al. (2006)			
Region	Mean Difference	Range of Difference	Difference σ	n
GOM	13	(-27) - 82	10	1539
GBN	4	(-32) - 67	10	1353
MAB	1	(-66) - 87	12	2764
SBF	-4	(-64) - 53	13	1919

Supplementary Material

Statistical Calculation Detail

Precision was determined as one standard deviation (σ) of repeated measurements of certified reference material (CRM):

$$\sigma = \pm\sqrt{\frac{\sum_{i=1}^{n}(TA_i - \overline{TA})^2}{n-1}} \quad (1)$$

where *n* is the number of measurements, TA_i is the i[th] of n TA measurements, and $\overline{TA}$ is the mean of all TA measurements. Accuracy was determined at the root mean square error (RMSE) of repeated CRM measurements relative to the certified TA, or of the TA differences of paired samples measured by independent instruments such as laboratory titration systems:

$$RMSE = \pm\sqrt{\frac{1}{n}\sum_{i=1}^{n}(TA_{A,i} - TA_{B,i})^2} \quad (2)$$

where *n* is the total number of paired sample or CRM measurements, $TA_{A,i}$ is the i[th] TA measured by instrument A, and $TA_{B,i}$ is either the i[th] TA measured by instrument B or the CRM TA concentration. The RMSE and CRM uncertainty were then used to calculate a total bias uncertainty *u(bias)*:

$$u(bias) = \pm\sqrt{RMSE^2 + u(CRM)^2} \quad (3)$$

where *u(CRM)* is the uncertainty of the certified CRM TA concentration. Then *u(bias)* and *σ*, together with a *u(other)* term for non-CRM seawater samples, were combined into an overall uncertainty u_c (approximating a 68.3% confidence interval):

$$u_c = \pm\sqrt{\sigma^2 + u(bias)^2} \quad (4)$$

The combined known uncertainties between the HydroFIA TA measurements and discrete TA measurements, with uncertainties calculated from replicate bottle analyses can be propagated into a combined uncertainty- $u_{c(HydroFIA\ TA,B)}$- as:

$$u_{c(HydroFIA\,TA,B)} = \pm\sqrt{u_{c(HydroFIA\,TA)}{}^2 + u_{c(B)}{}^2 + u(rep) + u(other)} \quad (5)$$

where *u(rep)* is calculated from Equation 4 (substituting the calculated RMSE of replicate bottle samples for u_c and *u(rep)* for *u(bias)*. The *u(other)* term includes all potential non-instrumental uncertainties, including temporal offsets between sample collection and instrument measurement times, discrete sample preservation uncertainties, and other unknown uncertainties.

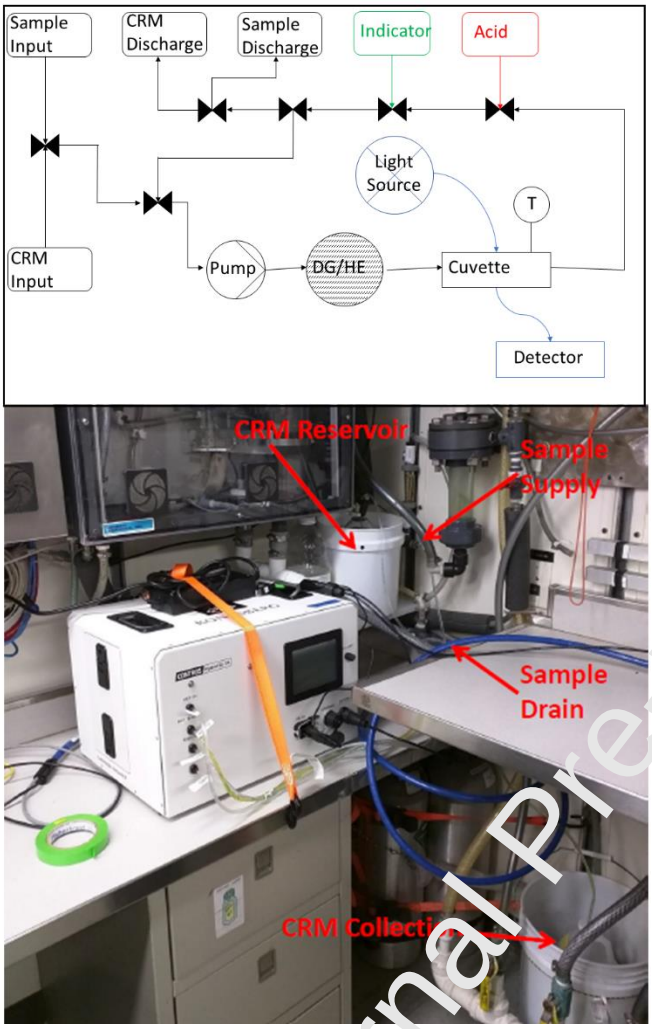

Figure S1. Top panel: schematic diagram of HydroFIA TA instrument components as used in this work, including modifications for automated CRM measurements. Bottom panel: photograph of the HydroFIA TA analyzer, installed aboard the NOAA Ship *Henry B. Bigelow*.

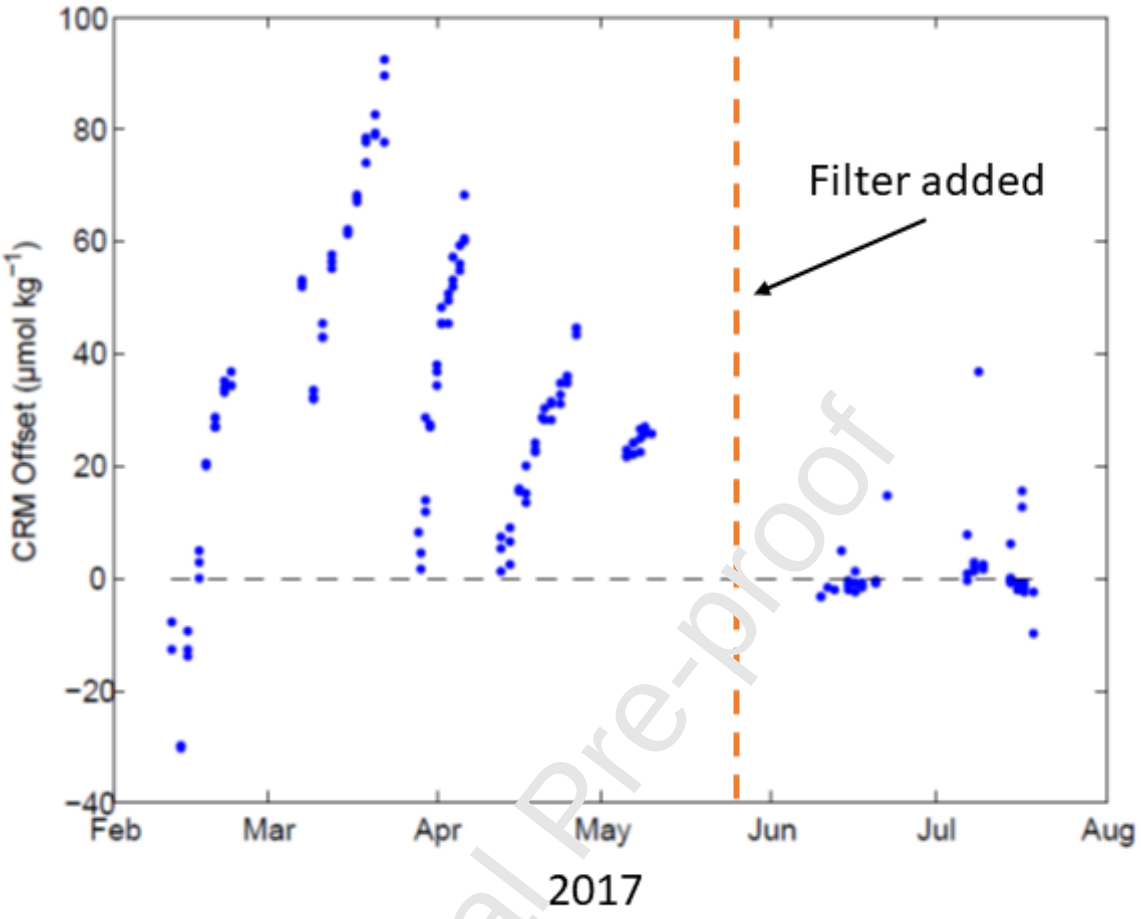

Figure S2. Offsets of automated HydroFIA TA measurements of certified reference material (CRM) measured during the seven 2017 cruises. The offset was calculated as the certified TA concentration subtracted from the measured TA value, thus positive values indicate an overestimate of the CRM TA. The CRM used on 2017 cruises was Batch 159, with a certified TA concentration of 2213.59 µmol kg^{-1} (Dickson et al. 2003). The in-line filter described in the text was added in June with some sample offsets (i.e. noise) but no substantial drift observed after.

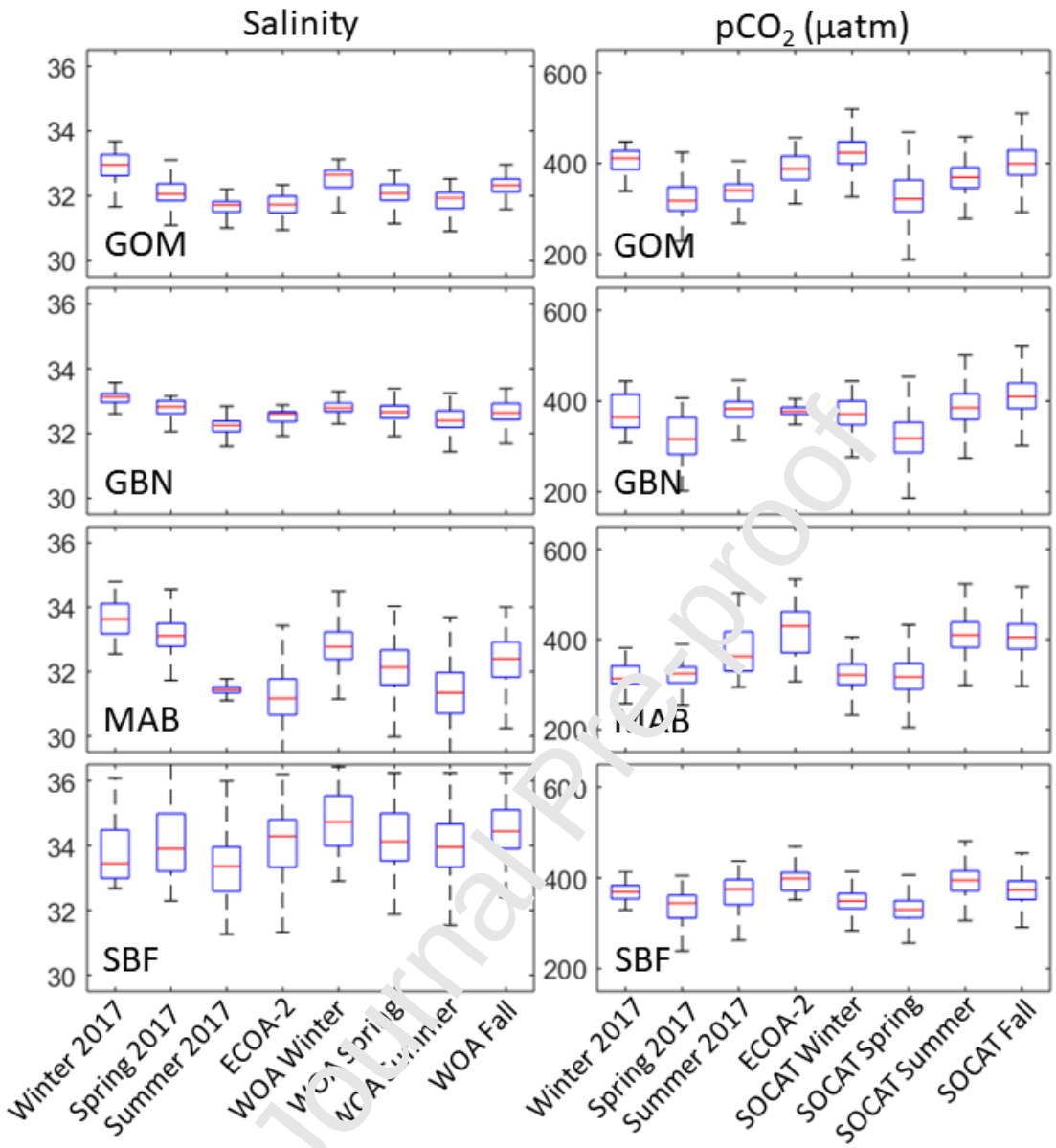

Figure S3. Seasonal box-and-whisker plots of mean salinity (left panels) and mean pCO_2 (right panels, µatm). Red lines denote mean values, upper and lower box boundaries depict the 75th and 25th percentiles, respectively, and whiskers depict range of values. WOA and SOCAT datasets are described in the text.

	Dates	Minimum CRM Offset (µmol kg-1)	Maximum CRM Offset (µmol kg-1)	Mean CRM Offset (µmol kg-1)	σ (µmol kg-1)	n
Cruise 1	Feb 11 - Feb 22	-31	37	11	6.2	27
Cruise 2	Mar 7 - Mar 22	32	93	62	2.5	27
Cruise 3	Mar 28 - Apr 6	2	68	39	3.4	27
Cruise 4	Apr 12 - Apr 26	1	45	24	1.2	30
Cruise 5	May 5 - May 11	22	27	24	1	18
Cruise 6	Jun 10 - Jun 22	-4	15	0	4.2	26
Cruise 7	Jul 6 - Jul 19	-10	37	5	3.3	38

Table S1. Summaries of automated Certified Reference Material tests aboard the *Bigelow* during cruises in 2017. The CRM used was Batch 159 (TA 2213.59 µmol kg^{-1} and salinity 33.572, Dickson et al. 2003). Plots of individual CRM tests are shown in Supplementary Figure S1. The offset was calculated as the certified TA concentration subtracted from the measured TA value, and thus positive values indicate an overestimate of the CRM TA by the HydroFIA TA instrument.

Table S2. Data sources used to compile the 'Historical' East Coast TA dataset described in this work.

Filename	region	source/link
33GG20130609_BT.csv	Gulf of Maine, Georges Bank, Mid-Atlantic Bight	https://www.aoml.noaa.gov/ocd/gcc/shortcruises/GU1302/GU1302-Discrete.csv
33GG20131114_BT.csv	Gulf of Maine, Georges Bank, Mid-Atlantic Bight	https://www.aoml.noaa.gov/ocd/gcc/shortcruises/GU1305/GU1305-Discrete.csv
33GG20140301_GU1401_hy1.csv	Gulf of Maine, Georges Bank, Mid-Atlantic Bight	https://www.aoml.noaa.gov/ocd/gcc/shortcruises/GU1401/GU1401-Discrete.csv
33GG20151012-GU1506-data.xlsx	Gulf of Maine, Georges Bank, Mid-Atlantic Bight	https://www.aoml.noaa.gov/ocd/gcc/shortcruises/GU1506/33GG20151012-GU1506-data
33GG20160521-GU1608-data.xls	Gulf of Maine, Georges Bank, Mid-Atlantic Bight	https://www.aoml.noaa.gov/ocd/gcc/shortcruises/GU1608/33GG20160521-GU1608-data
33GG20160521-GU1608-data.xls	Gulf of Maine, Georges Bank, Mid-Atlantic Bight	https://www.aoml.noaa.gov/ocd/gcc/shortcruises/GU1608/33GG20160521-GU1608-data
33GG20170516_GU1701_GU1702_data.xls	Gulf of Maine, Georges Bank, Mid-Atlantic Bight	http://www.aoml.noaa.gov/ocd/gcc/shortcruises/GU1701/33GG20170516-GU1701-data.

33GG20170610-GU1702-data.csv	Gulf of Maine, Georges Bank, Mid-Atlantic Bight	http://www.aoml.noaa.gov/ocd/gcc/shortcruises/GU1702/33GG20170610-GU1702-data.
33GG20171031-GU1706-data.csv	Gulf of Maine, Georges Bank, Mid-Atlantic Bight	http://www.aoml.noaa.gov/ocd/gcc/shortcruises/GU1706/33GG20171031-GU1706-data.
33GG20180822-GU1804-data.csv	Gulf of Maine, Georges Bank, Mid-Atlantic Bight	http://www.aoml.noaa.gov/ocd/gcc/shortcruises/GU1804/33GG20180822-GU1804-data.
33HH20140902-HB_1405-data.csv	Gulf of Maine, Georges Bank, Mid-Atlantic Bight	https://www.aoml.noaa.gov/ocd/gcc/shortcruises/HB1103/Bigelow_1103-Discrete-Web.c
Bigelow_1103-Discrete-Web.csv	Gulf of Maine, Georges Bank, Mid-Atlantic Bight	https://www.aoml.noaa.gov/ocd/gcc/shortcruises/HB1103/Bigelow_1103-Discrete-Web.c
33HH20120531-HB1202-data.csv	Gulf of Maine, Georges Bank, Mid-Atlantic Bight	https://www.aoml.noaa.gov/ocd/gcc/shortcruises/HB1202/33HH20120531-HB1202-data.
33HH20130314-HB1301-data.xlsx	Gulf of Maine, Georges Bank, Mid-Atlantic Bight	https://www.aoml.noaa.gov/ocd/gcc/shortcruises/HB1301/33HH20130314-HB1301-data.
33HH20140902-HB_1405-data.csv	Gulf of Maine, Georges Bank, Mid-Atlantic Bight	https://www.aoml.noaa.gov/ocd/gcc/shortcruises/HB1405/33HH20140902-HB_1405-dat
33HH20150519-HB1502-data.csv	Gulf of Maine, Georges Bank, Mid-Atlantic Bight	https://www.aoml.noaa.gov/ocd/gcc/shortcruises/HB1502/33HH20150519-HB1502-data.
33HH20170210-HB1701-data.xls	Gulf of Maine, Georges Bank, Mid-Atlantic Bight	https://www.aoml.noaa.gov/ocd/gcc/shortcruises/HB1701/33HH20170210-HB1701-data.

33HH20180523-HB1803-data.csv	Gulf of Maine, Georges Bank, Mid-Atlantic Bight	http://www.aoml.noaa.gov/ocd/gcc/shortcruises/HB1803/33HH20180523-HB1803-data.c
33H520181102-S11802-data.csv	North Atlantic	https://www.aoml.noaa.gov/ocd/gcc/shortcruises/Delaware_II_1202/Delaware_1202-Dis
46SL20181115-Transit846-data.csv	North Atlantic	http://www.aoml.noaa.gov/ocd/gcc/shortcruises/Selfoss/46SL20181115-Transit846-data.
Reykjafoss_2010-Discrete-Web.csv	North Atlantic	https://www.aoml.noaa.gov/ocd/gcc/shortcruises/Reykjafoss_2010/Reykjafoss_2010-Dis
PC1207-Discrete.csv	Mid Atlantic	https://www.aoml.noaa.gov/ocd/gcc/shortcruises/PC1207/PC1207-Discrete.csv
PC1405-Discrete.csv	Mid Atlantic	https://www.aoml.noaa.gov/ocd/gcc/shortcruises/PC1405/PC1405-Discrete.csv
PC1607-PC1609-data.xls	Mid Atlantic	https://www.aoml.noaa.gov/ocd/gcc/shortcruises/PC1607_PC1609/PC1607-PC1609-data
MLCE-EQUINOX-2015-2016-Data.csv	Mid Atlantic	https://www.aoml.noaa.gov/ocd/gcc/shortcruises/EQNX_2015_2016/MLCE-EQUINOX-20
GOMECC1MasterBottle06212013.xls	East Coast	https://www.aoml.noaa.gov/ocd/gcc/GOMECC1/data.php
GOMECC2_discrete_underway_samples.xlsx	East Coast	https://www.aoml.noaa.gov/ocd/gcc/GOMECC2/GOMECC2_discrete_underway_samples
GOMECC2_station_data.xlsx	East Coast	https://www.aoml.noaa.gov/ocd/gcc/GOMECC2/GOMECC2_station_data_version4.xlsx
ECOA2015_Discrete_Underway_Data_Final.xlsx	East Coast	https://www.nodc.noaa.gov/oads/data/0157389.xml
ECOA2015_MasterSamplingSheet_vAlk.xlsx	East Coast	https://www.nodc.noaa.gov/oads/data/0157389.xml
BioChem_Query_1801_Data.csv	Northeast, Canadian Maritimes, Labrador Sea	http://www.dfo-mpo.gc.ca/science/data-donnees/biochem/index-eng.html
bats_bottle.xls	Sargasso Sea	http://batsftp.bios.edu/BATS/bottle/bats_bottle.txt
GLODAP	Atlantic	https://www.nodc.noaa.gov/archive/arc0133/0186803/2.2/data/0-data/
OMP	East Coast	Charles Flagg, Pers. Comm.

Highlights

- Automated total alkalinity (TA) analyses greatly expanded spatiotemporal coverage
- Regional distributions of TA relative to salinity changed between seasons and years
- Seasonal changes were sometimes inconsistent with a new historical dataset